and rapid cooling. One hundred μl of 1 mol/l HCl and 2.5 μl of 0.4 mmol/l 5β-cholanic acid 3α, 6β-diol ethanol solution (Internal standard of HPLC) were added, and centrifuged at 2000 ×*g* for 10 min under 4 °C condition. The supernatant was collected and dried at 37 °C under N_2 gas, and then dissolved in 50% ethanol. The concentrations of HDCA, MDCA and CDCA were measured by HPLC and these velocities were calculated.

2.6. Analysis of mRNA levels

Messenger RNA (mRNA) levels of differentially expressed genes were analyzed using reverse transcription-polymerase chain reaction (RT-PCR). Single-strand cDNAs were constructed using an oligo (dT) primer with the Ready-to-Go You-Prime First-strand Beads kit (GE Healthcare UK Ltd, Buckinghamshire, UK). These cDNAs provided templates for PCRs using specific primers at a denaturation temperature of 94 °C for 30 s, an annealing temperature of 58 °C for 30 s, and an elongation temperature of 72 °C for 30 s in the presence of deoxynucleoside-5′-triphosphates and Taq polymerase. The PCR cycle numbers were titrated for each primer pair to ensure amplification in linear range. The reaction was completed by 7 min incubation at 72 °C. PCR products were analyzed in 2% agarose gel (w/v) containing ethidium bromide for visualization. The specific forward and reverse primers for the genes examined by PCR are shown in Table 1. These mRNA levels were normalized from Glyceraldehyde-3-phosphate-dehydrogenase (GAPDH) mRNA levels.

2.7. Statistical analysis

All data are shown as the mean±S.D. Statistically significant differences among groups were assessed by ANOVA followed by Dunnet's multiple comparison with the SAS software (SAS Institute Inc., Cary, NC). Probability values of less than 0.05 were considered to be statistically significant.

3. Results

3.1. Influence of ME3738 administration on LCA-induced hepatotoxicity

Plasma alanine aminotransferase (ALT) and alkaline phosphatase (ALP) activities were increased to 643 and 349 IU/l, respectively, following LCA treatment, which suggested that severe hepatotoxicity and cholestasis were induced in the mice. In contrast, co-administration with 0.05 and 0.15% ME3738 significantly reduced LCA-induced ALT by 35 and 38% and ALP by 46 and 50%, respectively (Fig. 1A and B). As well as ALT and ALP activities, the hepatic bile acid concentration was increased in LCA-treated mice. The concentration in LCA-treated mice was approximately 13-fold higher than that in control mice (Fig. 1C). Co-administration with ME3738 reversed the elevation of concentrations, as compared with LCA-treated mice. These data indicate that ME3738 lowers the elevation of hepatic bile acid concentrations and protects against LCA-induced hepatotoxicity.

Table 2
Hepatic bile acid composition (A) and biliary bile acid output (B)

	βMCA	TβMCA	UDCA	TUDCA	CA	TCA	CDCA	TCDCA	DCA	TDCA	LCA	TLCA
(A) Liver concentration (μmol/g liver)												
Control	0.02±0.02 (0.18)	N.D.	N.D.	N.D.	N.D.	0.09±0.03 (0.82)	N.D.	N.D.	N.D.	N.D.	N.D.	N.D.
ME3738	0.01±0.01 (0.11)	N.D.	N.D.	N.D.	N.D.	0.08±0.02 (0.89)	N.D.	N.D.	N.D.	N.D.	N.D.	N.D.
LCA	N.D.	N.D.	N.D.	N.D.	N.D.	0.17±0.02 (0.14)	N.D.	0.23±0.09 (0.19)	N.D.	0.02±0.01 (0.02)	N.D.	0.82±0.31 (0.66)
LCA +0.05% ME3738	N.D.	N.D.	N.D.	N.D.	N.D.	0.13±0.05 (0.15)	N.D.	0.18±0.11 (0.21)	N.D.	0.01±0.01 (0.01)	N.D.	0.56±0.24 (0.64)
LCA+0.15% ME3738	N.D.	N.D.	N.D.	N.D.	N.D.	0.13±0.04 (0.18)	N.D.	0.16±0.06 (0.23)	N.D.	0.01±0.01 (0.01)	N.D.	0.42±0.21 (0.59)
(B) Biliary output (μmol/min/kgw)												
Control	N.D.	0.22±0.06 (0.11)	N.D.	0.02±0.00 (0.01)	N.D.	1.65±0.37 (0.86)	N.D.	0.01±0.00 (0.01)	N.D.	0.02±0.00 (0.01)	N.D.	N.D.
ME3738	N.D.	0.37±0.04 (0.11)	N.D.	0.04±0.01 (0.01)	N.D.	2.23±0.25 (0.83)	N.D.	0.02±0.00 (0.01)	N.D.	0.02±0.01 (0.01)	N.D.	N.D.
LCA	N.D.	0.17±0.10 (0.11)	N.D.	N.D.	N.D.	0.43±0.18 (0.27)	N.D.	0.69±0.21 (0.43)	N.D.	0.04±0.01 (0.03)	N.D.	0.25±0.05 (0.16)
LCA +0.05% ME3738	N.D.	0.15±0.08 (0.04)	N.D.	0.02±0.02 (0.01)	N.D.	1.22±0.73 (0.34)	N.D.	1.58±0.66 (0.44)	N.D.	0.02±0.01 (0.01)	N.D.	0.59±0.29 (0.16)
LCA +0.15% ME3738	N.D.	0.48±0.24 (0.10)	N.D.	N.D.	N.D.	1.14±0.74 (0.25)	N.D.	2.00±0.81 (0.43)	0.01±0.01 (0.00)	0.16±0.14 (0.03)	N.D.	0.80±0.46 (0.17)

Hepatic and biliary bile acid compositions were determined by HPLC. Liver homogenates were prepared and bile was collected from C57BL/6N mice fed a control, 0.15% ME3738, 0.75% LCA, LCA+0.05% ME3738 or LCA+0.15% ME3738 diet for 6 days. Data are shown as the mean±S.D. ($n=5$). N.D. of liver concentration and biliary output represents below 0.01 μmol/g liver and 0.01 μmol/min/kgw, respectively. Numbers in parenthesis represent % of the total bile acids. βMCA; β-Muricholate, TβMCA; Tauro-β-muricholate, UDCA; Ursodeoxycholate, TUDCA; Tauroursodeoxycholate, CA; Cholate, TCA; Taurocholate, CDCA; Chenodeoxycholate, TCDCA; Taurochenodeoxycholate, DCA; Deoxycholate, TDCA; Taurodeoxycholate, LCA; Lithocholate, TLCA; Taurolithocholate.

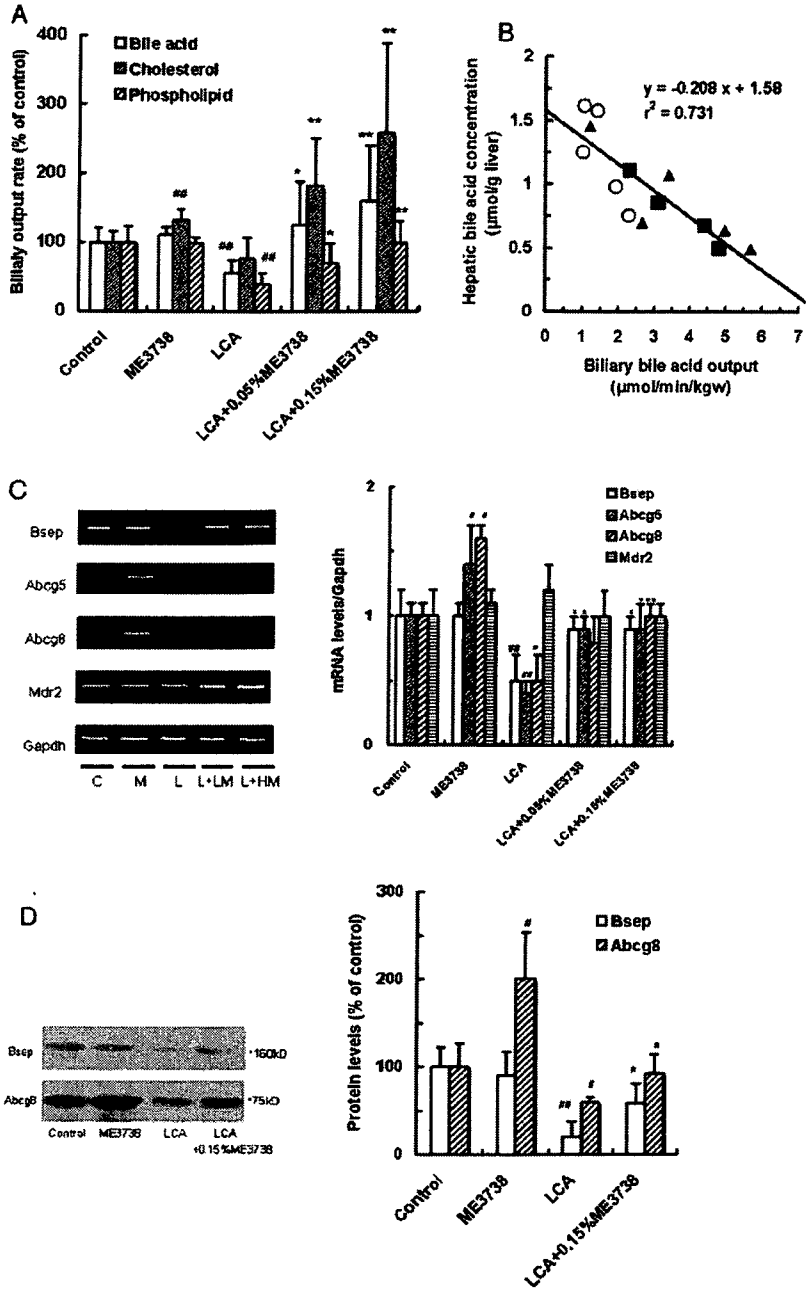

Fig. 3. Biliary bile acid, cholesterol and phospholipid outputs (A), correlation between biliary bile acid output and hepatic bile acid concentration (B), hepatic expression of transporter-related genes (C), and bile salt export pump (Bsep) and ATP-binding cassette g8 (Abcg8) protein levels (D). A) The bile was collected for 30 min by bile duct cannulation from C57BL/6N mice fed a control, 0.15% ME3738, 0.75% LCA, LCA+0.05% ME3738 or LCA+0.15% ME3738 diet for 6 days. Biliary bile acid, cholesterol and phospholipid concentrations were measured by enzyme-colorimetric method. B) Liver homogenate was prepared from C57BL/6N mice fed a 0.75% LCA (open circle), LCA+0.05% ME3738 (closed triangle) or LCA+0.15% ME3738 (closed square) diet for 6 days. The hepatic bile acid concentration was measured by enzyme-colorimetric method. C) Hepatic mRNAs were prepared from C57BL/6N mice fed a control (C), 0.15% ME3738 (M), 0.75% LCA (L), LCA+0.05% ME3738 (L+LM) or LCA+0.15% ME3738 (L+HM) diet for 6 days. The hepatic mRNA levels were measured by RT-PCR. Specific primers represented in Table 1. D) Bsep and Abcg8 protein levels were measured by Western blot analysis. Plasma membrane proteins were subjected to sodium dodecyl sulfate-polyacrylamide gels and electrically transferred to nitrocellulose membranes for immuno-staining with anti-mouse Bsep and anti-human Abcg8 antibody. Data are shown as the mean±S.D. (n=4). $^{\#}$, $^{\#\#}$ Significantly different from control group ($P<0.05$, $P<0.01$, respectively). *, ** Significantly different from LCA group ($P<0.05$, $P<0.01$, respectively).

3.2. Hepatic hydroxysteroid sulfotransferase 2a protein levels

LCA sulfation by hydroxysteroid sulfotransferase 2a has been reported to be involved in the protection against LCA-induced hepatotoxicity. The hepatic hydroxysteroid sulfotransferase 2a protein level, however, was not clearly different between control and ME3738-treated mice (Fig. 2A). The protein level increased by 1.7-fold in LCA-treated mice, as

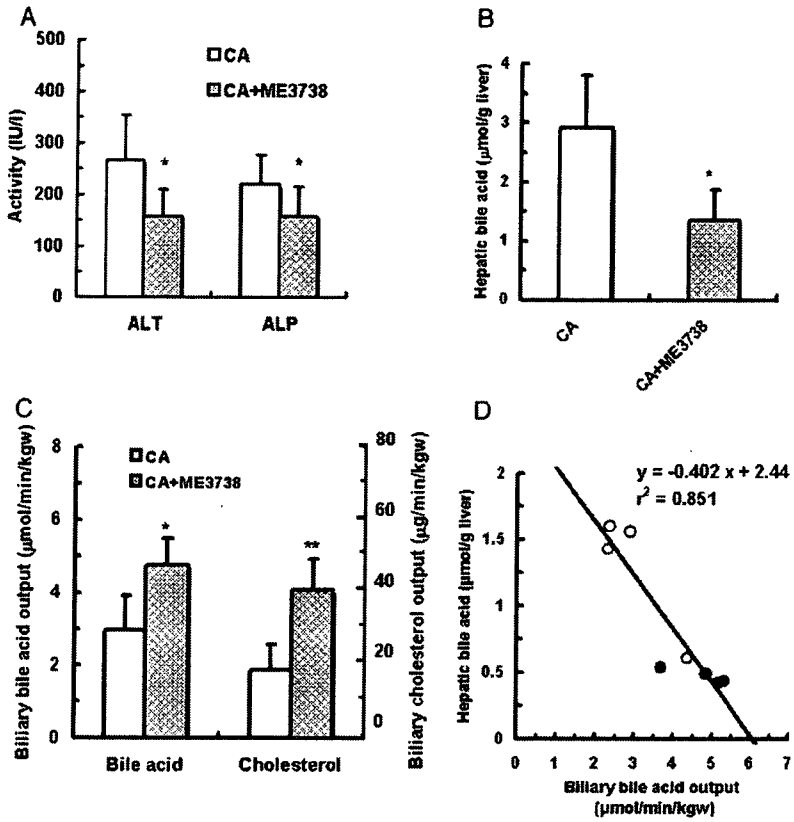

Fig. 4. Plasma alanine aminotransferase (ALT) and alkaline phosphatase (ALP) activities (A), hepatic bile acid level (B), biliary cholesterol and bile acid outputs (C), correlation between biliary bile acid output and hepatic bile acid concentration (D) in farnesoid X receptor-null mice fed a 0.25% cholate (CA) or CA + 0.15% ME3738 diet. Plasma and liver homogenates were prepared from farnesoid X receptor-null mice fed a CA or CA + 0.15% ME3738 diet for 6 days. A) Plasma ALT and ALP activities were measured by enzyme-colorimetric method. B) Hepatic bile acid concentration was measured by enzyme-colorimetric method. C) The bile was collected for 30 min by bile duct cannulation. Biliary bile acid and cholesterol concentrations were measured by enzyme-colorimetric method. D) Plots represent CA-treated mice (open circle) and CA + ME3738 treated mice (closed circle). Data are shown as the mean ± S.D. (n=3–5). *,** Significantly different from the CA group ($P<0.05$, $P<0.01$, respectively).

compared with that in the control mice. No clear enhancement in the hepatic hydroxysteroid sulfotransferase 2a protein level was observed in mice co-treated with ME3738 and LCA, as compared with LCA-treated mice.

3.3. LCA hydroxylase activities

LCA is mainly oxidized to produce 6α-, 6β- and 7α-hydroxy derivatives (Zimniak et al., 1989). Therefore, 6α-, 6β- and 7α-hydroxylase activities of LCA were measured using liver microsomes prepared from the control and ME3738-treated C57BL/6N mice. The 6α-, 6β- and 7α-hydroxylase activities were not significantly different between the control and ME3738-treated mice (Fig. 2B). The 6β-hydroxylase activity was approximately 20- to 30-fold higher than 6α- and 7α-hydroxylase activities. This result is consistent with the data from Zimniak et al.

3.4. Hepatic and biliary bile acid composition

To determine the influence of ME3738 administration on bile acid composition, the hepatic and biliary bile acid levels were measured in mice that were fed a control diet or a diet supplemented with ME3738, LCA or LCA+ME3738. No obvious changes in hepatic and biliary bile acid compositions were observed in ME3738-treated mice, as compared with the control mice. Hepatic tauroLCA (TLCA), taurochenodeoxycholate (TCDCA) and taurocholate (TCA) concentrations were, however, increased in the LCA-treated mice, whereas ME3738 co-treatment reversed the increase in these bile acid levels in a dose-dependent manner (Table 2). Biliary TLCA, TCDCA and TCA outputs were decreased in LCA-treated mice, whereas ME3738 co-treatment retrieved the decrease in biliary bile acid output in a dose-dependent manner (Table 2). No obvious changes in hepatic and biliary bile acid compositions were also observed in LCA+ME3738-treated mice, as compared with LCA-treated mice.

3.5. Bile flow, and biliary bile acid, cholesterol and phospholipid output

We measured bile flow rate, initially. The bile flow rate in mice fed a control, ME3738, LCA, LCA+0.05% ME3738 or LCA+0.15% ME3738 diet was 94.2± 13.3, 95.7 ± 5.1, 52.9±

14.4, 101.4± 37.5 and 115.5± 20.3 μl/min/kgw, respectively. The rate was significantly decreased in LCA-treated mice, compared with that in control mice ($P<0.01$). Bile is known to consist mainly of bile acid, cholesterol and phospholipid. We therefore considered that the mechanism of hepatic bile acid reduction by ME3738 was involved in biliary outputs of bile acid, cholesterol and phospholipid. Their outputs were decreased in LCA-treated mice. In contrast, co-administration of ME3738 increased them (Fig. 3A). ME3738 administration alone resulted in an increase in biliary output of cholesterol but not increases in biliary bile acid and phospholipids outputs. Biliary output of cholesterol was enhanced by ME3738 administration alone by approximately 1.5-fold.

3.6. Inverse correlation between biliary bile acid output and hepatic bile acid concentration

Co-administration of ME3738 increased biliary bile acid output and decreased hepatic bile acid concentration in LCA-treated mice. Therefore, a correlation between biliary bile acid output and hepatic bile acid concentration was determined. A clear inverse correlation ($r^2=0.731$) between them was observed in LCA- and LCA+ME3738-treated mice (Fig. 3B).

3.7. Hepatic mRNA levels

Biliary excretion of bile acid, cholesterol and phospholipid is mediated by bile salt export pump, ATP-binding cassette g5/8 and multi-drug resistance protein 2 (Mdr2), respectively. To assess changes in these gene expressions, we measured the expression levels of these transporters by RT-PCR. Consistent with the biliary cholesterol output, hepatic ATP-binding cassette g5 and g8 mRNA levels were increased significantly by 1.4- and 1.6-fold, respectively, in ME3738-treated mice. In LCA-treated mice, hepatic ATP-binding cassette g5/8 and bile salt export pump mRNA levels were decreased, and no clear changes were detected in the multi-drug resistance protein 2 mRNA level. The hepatic ATP-binding cassette g5, g8 and bile salt export pump mRNA levels in LCA+0.15% ME3738-treated mice were 2.3-, 2.0- and 1.8-fold higher than those in LCA-treated mice, respectively (Fig. 3C).

3.8. Hepatic bile salt export pump and ATP-binding cassette g8 protein levels

The hepatic bile salt export pump and ATP-binding cassette g5/8 mRNA levels were increased in LCA+ME3738-treated mice, as compared to those in LCA-treated mice. Thus, the hepatic bile salt export pump and ATP-binding cassette g8 protein levels were also measured. The former one was not enhanced, whereas the latter one was increased significantly in ME3738-treated mice (Fig. 3D). The hepatic bile salt export pump and ATP-binding cassette g8 protein levels were reduced to 20 and 60% of the control in LCA-treated mice, respectively. In LCA+ME3738-treated mice, these protein levels were enhanced by 2.9- and 1.5-fold, respectively, as compared to those in LCA-treated mice.

3.9. Influence of ME3738 administration on cholate-treated farnesoid X receptor-null mice

In order to assess whether ME3738 protects against hepatotoxicity in another mouse model that is independent of bile acid metabolism, we chose the cholate (CA)-treated farnesoid X receptor-null mouse model.

Plasma ALT and ALP activities were increased to 266 and 220 IU/l, respectively, in CA-treated farnesoid X receptor-null mice. Co-treatment with ME3738 significantly decreased both activities to 158 IU/l (Fig. 4A). Consistent with plasma diagnosis parameters, hepatic bile acid concentrations in farnesoid X receptor-null mice that were co-treated with ME3738 were lower than those in the mice treated with CA (Fig. 4B). Bile flow rate in CA and CA+ME3738 treated farnesoid X receptor-null mice was 73.7± 21.8 and 94.6± 7.3 μl/min/kgw, respectively. Biliary outputs of bile acid and cholesterol were increased up to 1.6- and 2.2-fold, respectively, in CA+ME3738-treated farnesoid X receptor-null mice, as compared with those in CA-treated farnesoid X receptor-null mice (Fig. 4C). A clear inverse correlation ($r^2=0.851$) between biliary bile acid output and hepatic bile acid concentration (Fig. 4D) was observed.

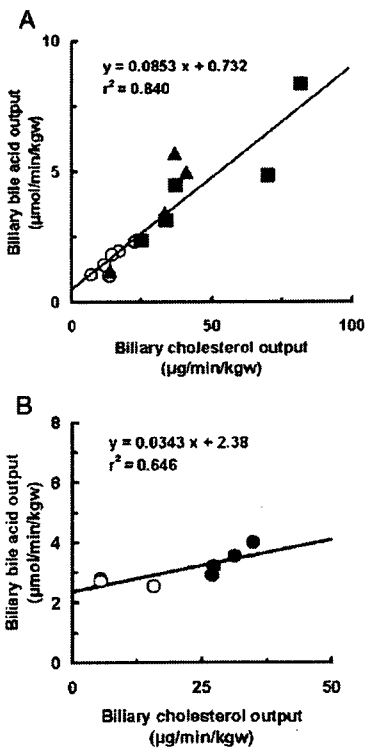

Fig. 5. Correlation between biliary outputs of cholesterol and bile acid. A) The bile was collected by bile duct cannulation from C57BL/6N mice fed a 0.75% LCA (open circle), LCA+0.05% ME3738 (closed triangle) or LCA+0.15% ME3738 (closed square) diet for 6 days. B) The bile was collected by bile duct cannulation from farnesoid X receptor-null mice fed a 0.25% CA (open circle) or CA+0.15% ME3738 (closed circle) diet for 6 days. Biliary bile acid and cholesterol concentrations were measured by enzyme-colorimetric method.

3.10. Correlation between biliary output of cholesterol and bile acid

ME3738 administration alone to C57BL/6N mice increased biliary cholesterol output, consistent with an increase in the hepatic ATP-binding cassette g8 protein level. In order to examine if an increase in biliary cholesterol output induces biliary bile acid output would in the bile acid-induced hepatotoxicity mouse model, the correlations between biliary output of bile acid and cholesterol were analyzed. Clear correlations ($r^2 = 0.840$ and 0.646) between them were observed in LCA- and CA-induced hepatotoxicity model mice, respectively (Fig. 5A and B).

4. Discussion

We aimed to investigate using LCA-treated mice whether ME3738 protected against a typical bile acid-induced hepatotoxicity. Co-administration of ME3738 decreased plasma alanine aminotransferase (ALT) and alkaline phosphatase (ALP) activities, and hepatic bile acid concentration in LCA-treated mice as expected. Co-administration of ME3738 also reversed the decrease in biliary bile acid output. These results suggest that ME3738-mediated enhancement of biliary bile acid output is involved in the protection against LCA-induced toxicity.

LCA sulfation by hydroxysteroid sulfotransferase 2a (Sonoda et al., 2002; Kitada et al., 2003) and LCA hydroxylation (Xie et al., 2001; Hofmann, 2004) have been reported to be involved in the protection against LCA-induced hepatotoxicity. Additionally, LCA is oxidized to 6α-, 6β- and 7α-hydroxy derivatives in rats. *In vivo* and *in vitro* studies have shown that 6β-hydroxylation is the predominant metabolism involved in tauroLCA detoxification in rats and mice, which leads to formation of non-cholestatic metabolites, like tauro-conjugates of murideoxycholic acid and β-muricholic acid (Zimniak et al., 1989; Dionne et al., 1994). A pregnane X receptor (*PXR*) ligand, pregnenolone 16α-carbonitrile (PCN) has been shown to prevent LCA-induced hepatotoxicity through enhancing *Cyp3a*, hydroxysteroid sulfotransferase 2a protein levels and leading to phase I and II detoxification of LCA (Selye, 1972; Xie et al., 2001; Miyata et al., 2006). Hydroxysteroid sulfotransferase 2a protein level and 6α-, 6β- and 7α-hydroxylation activities of LCA were not significantly enhanced in ME3738-treated mice (Fig. 2A and B). Additionally, the hepatic *Cyp3a* protein level measured by Western blot analysis was not significantly different between LCA- and LCA+ME3738-treated mice (data not shown). Furthermore, hepatic and biliary bile acid compositions were not clearly different between LCA- and LCA+ME3738-treated mice (Table 2). These results suggested that ME3738 protected against LCA-induced hepatotoxicity through the mechanism independent of LCA sulfation and hydroxylation. Instead of phase I and II detoxification of LCA, co-treatment with ME3738 increased biliary bile acid output consistent with the hepatic bile salt export pump protein level, compared to LCA-treated mice.

A canalicular secretion of bile acid is the rate-limiting step in their overall transport from blood to bile, and mainly mediated by bile salt export pump. Crocenzi et al. reported that tauroLCA induced internalization of bile salt export pump into a cytosolic vesicular compartment in isolated rat hepatocyte couplet (Crocenzi et al., 2003). This report suggested that an increase in hepatic bile salt export pump protein level is one of the protective roles in the LCA-induced hepatotoxicity through an increase in biliary bile acid output. Thus, the retrieval of bile salt export pump protein level by co-administration of ME3738 might be involved in the protection against LCA-induced hepatotoxicity.

In order to identify the ME3738-mediated protective mechanisms for bile acid-induced hepatotoxicity, we also used a hepatotoxicity model of CA-treated farnesoid X receptor-null mice that are scarcely dependent on bile acid sulfation and oxidation. ME3738 also protected against the hepatotoxicity in this model. In two bile acid-induced hepatotoxicity models, co-treatment with ME3738 decreased hepatic bile acid concentration and increased biliary output of bile acid, and clear correlations between them were observed (Figs. 3B and 4D). These results suggested that ME3738 protected against LCA- and CA-induced hepatotoxicity through the decrease in hepatic bile acid concentration resulting from the increase in biliary bile acid output.

ME3738 treatment alone increased biliary output of cholesterol, consistent with the increase in hepatic ATP-binding cassette g8 protein level. Additionally, a clear correlation between the biliary outputs of cholesterol and bile acid was observed in LCA- and CA-induced hepatotoxicity mouse models (Fig. 5A and B). These results suggested the possibility that the protection mechanism of ME3738 against LCA- and CA-treated hepatotoxicity was relevant to the increase in biliary cholesterol output, consistent with the hepatic ATP-binding cassette g8 protein level. Several reports have suggested that the increased biliary cholesterol output enhanced biliary bile acid output. As an example, the treatment of rats and mice with a plant sterol, diosgenin, was shown to enhance biliary output of cholesterol without enhancing the biliary outputs of phospholipid and bile acid (Puglielli et al., 1994; Kamisako and Ogawa, 2003; Yamaguchi et al., 2003; Kamisako and Ogawa, 2005; Kosters et al., 2005). Biliary outputs of both cholesterol and bile acids were, however, increased in the diosgenin-pretreated rats as compared with those in the control rats, when TCA or tauroUDCA were infused to rats intravenously (Amigo et al., 1999; Kosters et al., 2005).

In the present study, we demonstrated that ME3738 protected LCA- and CA-induced hepatotoxicity. Our data suggest that ME3738 protects against LCA- and CA-induced hepatotoxicity by increased biliary bile acid output that is related to cholesterol output, and not by bile acid metabolism.

Acknowledgements

We would like to express our sincere thanks to Dr. Tsutomu Matsubara, Dr. Kiyoshi Nagata, Ms. Mariko Takagi and Dr. Shoji Nishiyama for skillful technical advice and support. This study was supported by a Grant-in-Aid from the Ministry of

Education, Science and Culture, Japan and by a Grant-in-Aid from the Ministry of Health, Labor and Welfare, Japan.

References

Amigo, L., Mendoza, H., Zanlungo, S., Miquel, J.F., Rigotti, A., Gonzalez, S., Nervi, F., 1999. Enrichment of canalicular membrane with cholesterol and sphingomyelin prevents bile salt-induced hepatic damage. J. Lipid Res. 40, 533–542.

Carey, J.B., Wilson, I.D., Zaki, F.G., Hanson, R.F., 1966. The metabolism of bile acids with special reference to liver injury. Medicine 45, 461–470.

Crocenzi, F.A., Mottino, A.D., Sanchez Pozzi, E.J., Pellegrino, J.M., Rodriguez Garay, E.A., Milkiewicz, P., Vore, M., Coleman, R., Roma, M.G., 2003. Impaired localisation and transport function of canalicular Bsep in taurolithocholate induced cholestasis in the rat. Gut 52, 1170–1177.

Dionne, S., Tuchweber, B., Plaa, G.L., Yousef, I.M., 1994. Phase I and phase II metabolism of lithocholic acid in hepatic acinar zone 3 necrosis. Evaluation in rats by combined radiochromatography and gas-liquid chromatography-mass spectrometry. Biochem. Pharmacol. 48, 1187–1197.

Fickert, P., Fuchsbichler, A., Marschall, H.U., Wagner, M., Zollner, G., Krause, R., Zatloukal, K., Jaeschke, H., Denk, H., Trauner, M., 2006. Lithocholic acid feeding induces segmental bile duct obstruction and destructive cholangitis in mice. Am. J. Pathol. 168, 410–422.

Fischer, S., Beuers, U., Spengler, U., Zwiebel, F.M., Koebe, H.G., 1996. Hepatic levels of bile acids in end-stage chronic cholestatic liver disease. Clin. Chim. Acta 251, 173–186.

Heuman, D.M., Pandak, W.M., Hylemon, P.B., Vlahcevic, Z.R., 1991. Conjugates of ursodeoxycholate protect against cytotoxicity of more hydrophobic bile salts: in vitro studies in rat hepatocytes and human erythrocytes. Hepatology 14, 920–926.

Hofmann, A.F., 2004. Detoxification of lithocholic acid, a toxic bile acid: relevance to drug hepatotoxicity. Drug Metab. Rev. 36, 703–722.

Honma, W., Shimada, M., Sasano, H., Ozawa, S., Miyata, M., Nagata, K., Ikeda, T., Yamazoe, Y., 2002. Phenol sulfotransferase, ST1A3, as the main enzyme catalyzing sulfation of troglitazone in human liver. Drug Metab. Dispos. 30, 944–949.

Jorquera, F., Monte, M.J., Guerra, J., Sanchez-Campos, S., Merayo, J.A., Olcóz, J.L., González-Gallego, J., Marin, J.J., 2005. Usefulness of combined measurement of serum bile acids and ferritin as additional prognostic markers to predict failure to reach sustained response to antiviral treatment in chronic hepatitis C. J. Gastroenterol. Hepatol. 20, 547–554.

Kamisako, T., Ogawa, H., 2003. Regulation of biliary cholesterol secretion is associated with abcg5 and abcg8 expressions in the rats: effects of diosgenin and ethinyl estradiol. Hepatol. Res. 26, 348–352.

Kamisako, T., Ogawa, H., 2005. Alteration of the expression of adenosine triphosphate-binding cassette transporters associated with bile acid and cholesterol transport in the rat liver and intestine during cholestasis. J Gastroenterol. Hepatol. 20, 1429–1434.

Kitada, H., Miyata, M., Nakamura, T., Tozawa, A., Honma, W., Shimada, M., Nagata, K., Sinal, C.J., Guo, G.L., Gonzalez, F.J., Yamazoe, Y., 2003. Protective role of hydroxysteroid sulfotransferase in lithocholic acid-induced liver toxicity. J. Biol. Chem. 278, 17838–17844.

Klein, C., Wustefeld, T., Heinrich, P.C., Streetz, K.L., Manns, M.P., Trautwein, C., 2003. ME3738 protects from concanavalin A-induced liver failure via an IL-6-dependent mechanism. Eur. J. Immunol. 33, 2251–2261.

Kosters, A., Frijters, R.J., Kunne, C., Vink, E., Schneiders, M.S., Schaap, F.G., Nibbering, C.P., Patel, S.B., Groen, A.K., 2005. Diosgenin-induced biliary cholesterol secretion in mice requires Abcg8. Hepatology 41, 141–150.

Kuzuhara, H., Nakano, Y., Yamashita, N., Imai, M., Kawamura, Y., Kurosawa, T., Nishiyama, S., 2006. Protective effects of alpha1-acid glycoprotein and serum amyloid A on concanavalin A-induced liver failure via interleukin-6 induction by ME3738. Eur. J. Pharmacol. 541, 205–210.

Meiji Seika Kaisha, Ltd., 2006. ME3738: Brochure of New Investigational Drug Information Package.

Miyata, M., Tozawa, A., Otsuka, H., Nakamura, T., Nagata, K., Gonzalez, F.J., Yamazoe, Y., 2005. Role of farnesoid X receptor in the enhancement of canalicular bile acid output and excretion of unconjugated bile acids: a mechanism for protection against cholic acid-induced liver toxicity. J. Pharmacol. Exp. Ther. 312, 759–766.

Miyata, M., Watase, H., Hori, W., Shimada, M., Nagata, K., Gonzalez, F.J., Yamazoe, Y., 2006. Role for enhanced faecal excretion of bile acid in hydroxysteroid sulfotransferase-mediated protection against lithocholic acid-induced liver toxicity. Xenobiotica 36, 631–644.

Puglielli, L., Amigo, L., Arrese, M., Nunez, L., Rigotti, A., Garrido, J., Gonzalez, S., Mingrone, G., Greco, A.V., Accatino, L., et al., 1994. Protective role of biliary cholesterol and phospholipid lamellae against bile acid-induced cell damage. Gastroenterology 107, 244–254.

Selye, H., 1972. Prevention by catatoxic steroids of lithocholic acid-induced biliary concrements in the rat. Proc. Soc. Exp. Biol. Med. 141, 555–558.

Shimada, M., Yoshinari, K., Tanabe, E., Shimakawa, E., Kobashi, M., Nagata, K., Yamazoe, Y., 2001. Identification of ST2A1 as a rat brain neurosteroid sulfotransferase mRNA. Brain Res. 920, 222–225.

Sinal, C.J., Tohkin, M., Miyata, M., Ward, J.M., Lambert, G., Gonzalez, F.J., 2000. Targeted disruption of the nuclear receptor FXR/BAR impairs bile acid and lipid homeostasis. Cell 102, 731–744.

Sonoda, J., Xie, W., Rosenfeld, J.M., Barwick, J.L., Guzelian, P.S., Evans, R.M., 2002. Regulation of a xenobiotic sulfonation cascade by nuclear pregnane X receptor (PXR). Proc. Natl. Acad. Sci. U. S. A. 99, 13801–13806.

Trauner, M., Arrese, M., Soroka, C.J., Ananthanarayanan, M., Koeppel, T.A., Schlosser, S.F., Suchy, F.J., Keppler, D., Boyer, J.L., 1997. The rat canalicular conjugate export pump (Mrp2) is down-regulated in intrahepatic and obstructive cholestasis. Gastroenterology 113, 255–264.

Xie, W., Radominska-Pandya, A., Shi, Y., Simon, C.M., Nelson, M.C., Ong, E.S., Waxman, D.J., Evans, R.M., 2001. An essential role for nuclear receptors SXR/PXR in detoxification of cholestatic bile acids. Proc. Natl. Acad. Sci. U. S. A. 98, 3375–3380.

Yamaguchi, A., Tazuma, S., Ochi, H., Chayama, K., 2003. Choleretic action of diosgenin is based upon the increases in canalicular membrane fluidity and transporter activity mediating bile acid independent bile flow. Hepatol. Res. 25, 287–295.

Yousef, I.M., Bouchard, G., Tuchweber, B., Plaa, G.L., 1997. Monohydroxy bile acid induced cholestasis: role of biotransformation. Drug Metab. Rev. 29, 167–181.

Zimniak, P., Holsztynska, E.J., Lester, R., Waxman, D.J., Radominska, A., 1989. Detoxification of lithocholic acid. Elucidation of the pathways of oxidative metabolism in rat liver microsomes. J. Lipid Res. 30, 907–918.

glycosaminoglycans (HSGs) are known to Ad5 receptors. We have previously developed mutant Ad vectors with ablation of CAR, αv integrins, and HSG binding by mutation of the FG loop in the fiber knob, deletion of the RGD motif of the penton base, and substitution of the fiber shaft domain for that derived from Ad type 35, respectively. In the present study, we examined the infectious mechanism of Ad vector in Caco-2 cell monolayer using the mutant Ad vectors. First, we examined the transgene expression in Caco-2 cell monolayer by conventional Ad vectors. Although Caco-2 cells differentiation into cell monolayer was followed by a decrease in the levels of transgene expression by conventional Ad vector. Next, we examined the comparison of transgene expression in Caco-2 cell monolayer by several mutant Ad vectors. Mutant Ad vectors with CAR or HSGs-binding ablation showed lower transgene expression than conventional Ad vector in Caco-2 cell monolayer. These results suggest that the CAR and HSGs-binding each plays an important role in Ad vector-mediated transduction to the Caco-2 cell monolayer.

54. INVOLVEMENTS OF *N*-HYDROXYLATION OF FLUTAMIDE METABOLITES AND HEPATIC GSH DEPLETION IN FLUTAMIDE-INDUCED HEPATOTOXICITY

Masato Ohbuchi[1], Masaaki Miyata[1], Daichi Nagai[2], Miki Shimada[1], Kouichi Yoshinari[1], and Yasushi Yamazoe[1]

[1]Graduate School of Pharmaceutical Sciences, Tohoku University, Sendai, Japan, [2]R&D Division, Pharmaceuticals Group, Nippon Kayaku Co., Ltd, Tokyo, Japan

Flutamide is a non-steroidal anti-androgen and clinically used for therapy of prostate cancer around the world. Severe liver injury has, however, been reported in patients treated with flutamide. Flutamide-induced liver toxicity had not been recognized during the development of this drug using experimental animals. The mechanism of the liver injury thus remains obscure until now. Flutamide is mainly hydrolyzed into an arylamine metabolite, 5-amino-2-nitrobenzotrifluoride (FLU-1), by carboxylesterase in both human and rodents. The involvement of toxic metabolites is suggested in flutamide-induced liver toxicity. Previously, *N*-hydroxylamine of FLU-1 (FLU-1 *N*-OH) was detected in the urine of patients as the glucuronide. Furthermore, the *N*-hydroxylamine showed a potent cytotoxicity in rat primary hepatocytes. So, FLU-1 is possible to mediate flutamide-induced liver injury in human. In the present study, we have investigated the mechanism of flutamide-induced liver injury from the aspect of drug metabolism using FLU-1 and TCPOBOP. C57BL/6N male mice were treated p.o. with FLU-1 (200 mg/kg body weight) for 5 days and i.p. with TCPOBOP (3 mg/kg body weight) for the first three days. Mice were fasted for the last two days to deplete hepatic glutathione (GSH). Cotreatment with FLU-1 and TCPOBOP significantly increased serum alanine aminotransferase activity (ALT) compared to the vehicle control. Treatment with FLU-1 or TCPOBOP alone did not increase serum ALT. Microsomal FLU-1 *N*-hydroxylation was measured by HPLC. Cotreatment with FLU-1 and TCPOBOP enhanced five-times the rate of microsomal FLU-1 *N*-hydroxylation, as well as observed after the treatment of TCPOBOP. Hepatic GSH levels were significantly reduced in FLU-1 and TCPOBOP cotreated mice compared to the vehicle control. In mice cotreated with FLU-1 and TCPOBOP, but not fasted, no influence on serum ALT and hepatic GSH levels were detected. These results suggest that both the hepatic production of FLU-1 *N*-OH and reduction of hepatic GSH are necessary prior to flutamide-induced liver injury in vivo.

医薬品開発における毒性評価のバイオマーカー

第一三共株式会社 安全性研究所
第七グループ長
矢本 敬

第一三共株式会社 安全性研究所
所長
真鍋 淳


矢本 敬


真鍋 淳

1—はじめに

バイオマーカー（biomarker）とは正常な生物学的プロセス、発病過程、あるいは薬物・化学物質曝露に対する薬理学的反応の指標として客観的に測定され評価される特性と定義される[1]。尿、血液、あるいは組織・器官等の生体由来の試料を用いて得られたデータは全てバイオマーカーとなり得る。医薬品開発においては尿検査、血液学的検査、血液化学的検査、病理学的検査から得られたデータが毒性評価のバイオマーカーとして従来より用いられている。例えば、肝障害の指標として血清ALT、AST、ビリルビンが、腎障害の指標として血清尿素窒素、クレアチニンが用いられ、病理組織学的変化も含めて毒性標的組織の確定と安全域の算出が実施されている。したがって、実験動物で再現可能な副作用に関しては、臨床試験開始前に十分なリスク評価とリスク管理が実施されている。一方、特異体質性薬剤障害は実験動物では予測不可能であり、臨床試験、あるいは市販後に初めてヒトでの副作用が明らかとなる。病態モデル動物や遺伝子改変動物を用いた毒性発現機作解明試験でも副作用を再現できないことがほとんどで、リスク評価とリスク管理のための新規の実験モデル開発やバイオマーカー探索が行われている。

近年の技術の進歩により、RNA、タンパク質、あるいは生体内代謝物を生物学的パラメータとして評価するための種々の分析ツールとしてマイクロアレイ、二次元電気泳動、LC-MSやNMR等の利用が可能となり、ヒトでのリスク評価のための毒性発現機作の解明やリスク管理のためのバイオマーカーの選択にも応用され始めている。これらのツールは生体由来試料より網羅的な情報を一斉に取得できることから、従来の検査方法では想定されていなかった新規バイオマーカーを検出できる可能性がある。本稿ではラットの酸化ストレス肝障害のモデルを主な例としてマイクロアレイ、二次元電気泳動、およびLC-MSを用いた遺伝子発現解析、タンパク質発現解析、内因性代謝物解析によるバイオマーカー探索とリスク評価について紹介する。

2—遺伝子発現解析
(Toxicogenomics：トキシコジェノミクス)

Stanford大学のBrownらは、1995年に複数のcDNAを基板にスポットして同時に定量する手法を開発し、さらに1996年にはヒトのcDNAを約1,000遺伝子搭載したDNAチップを作製した[2]。このマイクロアレイ技術は、多数の遺伝子の発現量を同時に定量することを可能とし、遺伝子塩基配列解読の進展とともにヒトの他、実験動物についても数千～数万遺伝子を搭載したマイクロアレイが現在市販されている。本稿ではAffymetrix社のGeneChipを用いた解析結果を基に紹介する。

アセトアミノフェン（APAP）は軽い発熱や頭痛等の症状を緩和する解熱鎮痛剤として用いられる薬物の主要成分の一つであり、標準的な用法・用量では非常に安全な薬物である。APAPは肝臓の薬物代謝酵素cytochrome P450によって高分子障害性の高い活性代謝物*N*-acetyl-*p*-benzoquinone imine（NAPQI）に代謝されるが、標準的な用法・用量ではNAPQIはglutathione S-transferaseにより速やかに無毒なグルタチオン抱合体となり胆汁中へと排泄される。しかし、APAPを大量に摂取した場合には肝臓中のグルタチオンが枯渇し、NAPQIが蓄積する。その結果、活性代謝物であるNAPQIはDNAやタンパク質とadductを形成し、肝障害を発現することとなる。グルタチオン枯渇がAPAPによる肝障害発現のキーとなっていることから、グルタチオン枯渇に関連する遺伝子群を選抜し、これらがAPAP類似の肝障害を引き起こす化合物の毒性を予測できるバイオマーカーとなり得るか検討した[3]。グルタチオン枯渇モデルとして肝臓でのグルタチオン生合成を阻害するL-buthionine (S, R)-sulfoximine (BSO) を

ラットに4日間飲水投与した。肝臓の遺伝子発現プロファイルをGeneChipシステムにより取得し、肝臓中グルタチオン濃度と逆相関した発現変動を示す遺伝子53個を抽出した。抽出した遺伝子セットを用いて主成分分析（PCA）を行った結果、成分1と2でBSOとAPAPが同じクラスターを形成し、酸化ストレスを惹起しない化合物と分離できた（**図1**）。これらの遺伝子セットは、化合物の酸化ストレスの有無を迅速かつ高感度にスクリーニングするためのバイオマーカーとして活用可能である。

また、毒性メカニズムの解明が進んでいるモデル化合物に関して構築された大規模遺伝子発現データベース（DB）を利用できれば、薬物代謝酵素関連遺伝子、細胞周期関連遺伝子、炎症反応関連遺伝子等のバイオマーカーを用いた階層的クラスタリング等により、評価化合物とモデル化合物との遺伝子発現プロファイルの類似性に基づいた毒性リスク予測・評価を行うことも可能になると期待される。大規模DB構築としては国内ではトキシコゲノミクス・インフォマティクスプロジェクト（TGP2、http://wwwtgp.nibio.go.jp/tgp2/index.html）が進行している。

マイクロアレイを用いた遺伝子発現解析では多数の遺伝子の発現量を同時に解析できることから、医薬品開発の毒性評価において現在では毒性バイオマーカーの探索のみならず、開発初期化合物のリスクの順位付け、あるいはヒトにおける毒性発現機作解明のためのフォローアップ試験等に幅広く応用されている。

3—タンパク質発現解析
(Toxicoproteomics：トキシコプロテオミクス)

タンパク質発現解析として、二次元電気泳動[1]、LC-MS、あるいはSELDI-TOF/MSによる組織、血液、尿中タンパク質の発現解析が報告されている。遺伝子情報から翻訳されたタンパク質はそのまま機能する場合のみではなく、リン酸化、糖鎖付加、あるいはスプライシング等の翻訳後修飾により機能する場合も多く、タンパク質発現解析は病態、あるいは生体の薬理学的反応を機能面から捉えるのに有用な手法である。しかしながら、試料の処理が煩雑であることや、検出感度の問題等により、遺伝子発現解析や内因性代謝物解析と比較するとスループットが低く大規模解析が困難である。したがって、遺伝子発現解析で選択された毒性バイオマーカーがタンパク質レベルでの機能とリンクしているか否かの検証や翻訳後修飾の有無の確認に用いることが実際的な応用であろう。本稿では二次元電気泳動とMALDI-TOF/MSを用いた解析結果を紹介する。

ペルオキシゾーム増生剤（PPAR）のclofibrate（CPIB）を投与したラット肝臓について二次元電気泳動を実施し、ペルオキシゾーム、ミトコンドリアに局在するタンパク質について解析を行い、遺伝子発現解析の結果と比較した。その結果、二次元電気泳動によりCPIBの薬理作用である脂質低下作用に関連する酵素の誘導が確認された。そのうち、げっ歯類特異的に

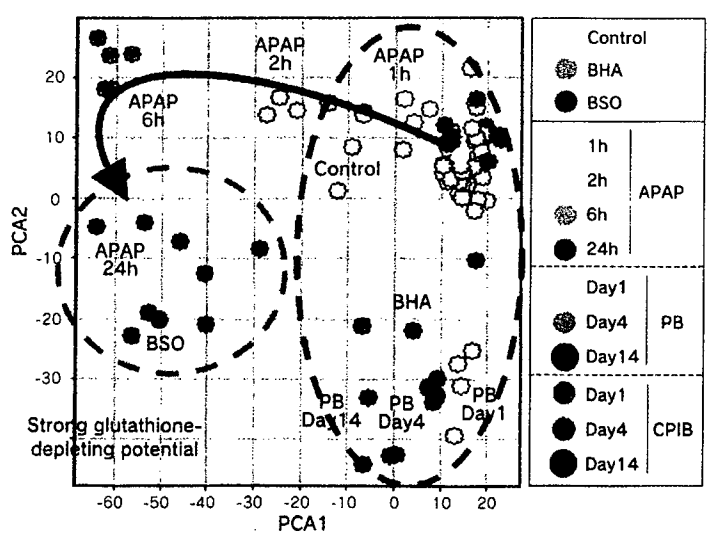

図1　グルタチオン枯渇関連遺伝子を用いた主成分分析

誘導される脂肪酸β-酸化酵素（acyl-CoA oxidase）がCPIB投与によりタンパク質レベルでも有意に増加した（図2）。

細胞骨格タンパク質であるkeratin 8は肝障害物質の曝露によりリン酸化が亢進することが知られている[9]。肝障害物質のbromobenzeneを投与したラット肝臓について二次元電気泳動を実施した結果、対照群と投与群の間で分子量がほぼ同じで等電点のみ異なるスポットが認められた。MALDI-TOF/MSを用いた同定により、両スポットとともにkeratin 8であることが確認され、抗リン酸化keratin 8抗体で標識した結果、投与群でリン酸化されたkeratin 8が増加していることが明らかとなった（図3）。

タンパク質発現解析は遺伝子発現解析が毒性バイオマーカーとして適切か否かの確認、あるいは生体の機能に重要な役割を果たしているリン酸化等の翻訳後修飾の確認に有用な手法であると言える。また、毒性バイオマーカーとしてタンパク質が同定された場合、その抗体を作製することで、その後のスクリーニング等に応用が可能となる。

4—内因性代謝物解析
(Toxicometabonomics：トキシコメタボノミクス)

生体では種々の代謝経路により内因性の代謝物が産生されており、化学物質の曝露により、これらの内因性代謝物量が変動することが知られている。トキシコメタボノミクスでは生体内で産生されるこれらの代謝物を網羅的に解析し、化学物質の曝露後の代謝物の量的変化から毒性機作の解明、リスク評価を行う。尿・血液等の比較的侵襲性の低い試料を検査対象とすることから、ヒトでの毒性バイオマーカーとしての有用性が期待されている。分析ツールとしては、NMR、あるいはLC-MSが汎用されている。Imperial College LondonのNicholsonらは^{1}H-NMRを用いたトキシコメタボノミクス・コンソーシアム（COMET）を欧米の企業5社と行っており、肝障害、腎障害のモデルとして80化

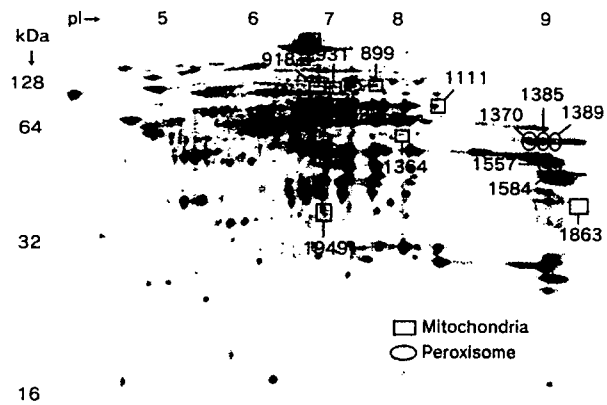

Tissue	Spot No.	Identified proteins	Expression	
			mRNA	Protein
Mitochondria	942	Methylcrotonoyl-CoA carboxylase 1 (alpha)		
	1370	3-hydroxy-3-methylglutaryl-CoA synthase 2		
	1385			
	1389			
	1557	Acetyl-CoA acyltransferase 2, mitochondrial		
	1584	Acetyl-CoA acetyltransferase 1		
Peroxisome	899	Acyl-CoA synthetase long-chain family member 1		
	918			
	931			
	1111	Catalase		
	1364	Acyl-CoA oxidase 1, palmitoyl		
	1863	Peroxisomal trans-2-enoyl-CoA reductase		
	1949	Enoyl-CoA hydratase 1, peroxisomal		

Not change　High

図2　二次元電気泳動とMALDI-TOF/MSによるPPARαアゴニストを投与したラット肝臓の解析結果

合物のデータを用いて尿中バイオマーカーを選抜し、肝毒性、腎毒性に対する特異性がそれぞれ77%と100%であると報告している[6]。また、慶應義塾大学先端生命科学研究所の曽我教授らはキャピラリー電気泳動－飛行時間型質量分析計（CE-TOF/MS）を用いたメタボノミクス解析を行い、APAPによるマウス肝障害モデルにおいて、肝臓および血清中で増加する内因性代謝物としてオフタルミン酸を同定している[7]。本稿ではAPAP、あるいはBSOを投与したラットの尿中バイオマーカーの探索を行った結果を紹介する。

APAPをラットに単回投与した後、24時間尿を採取した。BSOは飲水で4日間投与し、3日目より24時間尿を採取した。採取した尿は4倍希釈した後、UPLC-TOF/MS（ウォーターズ）を用いて解析を行った。対照群で検出された約1,400個のピークのうち、血清ALTレベルと相関する変動を示した175個のピークについてPCAを行った結果、成分1と2でALTの上昇に相関したクラスターを得ることができた（図4A）。さらに、肝臓中グルタチオン量と逆相関する変動を示した105個のピークを用いてAPAP投与群とBSO投与群のPCAを行った結果、APAPで肝障害を発現した投与群はBSO投与群と同じクラスターを形成し、遺伝子発現解析のみならず、メタボノミクス解析においてもグルタチオン枯渇モデルがAPAPによる酸化ストレス肝障害を予測できることが明らかとなった（図4B）。クラスタリングに強く寄与しているいくつかのピークにつ

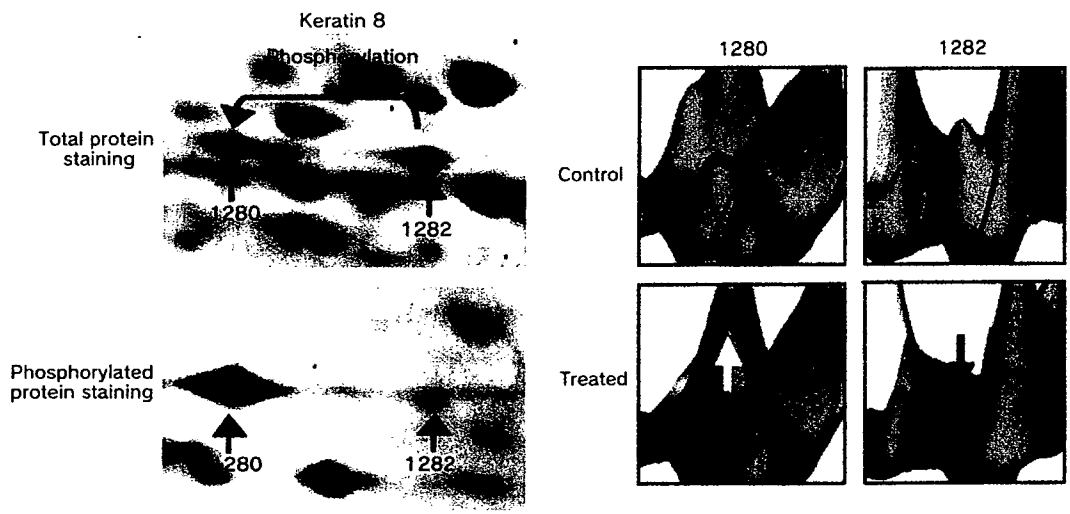

図3　二次元電気泳動、MALDI-TOF/MS、Western blotによるリン酸化keratin 8の同定結果

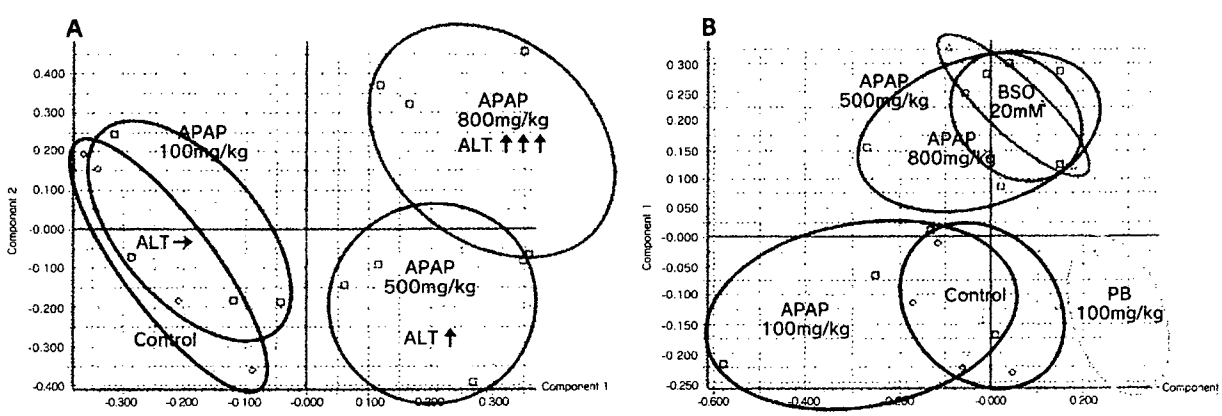

A 血清ALTと相関するピークを用いた主成分分析結果

B BSO投与で肝グルタチオン量と逆相関したピークを用いた主成分分析結果

図4　アセトアミノフェンを投与したラット尿のUPLC-MS解析例

いて現在同定を行っている。

NMR、あるいはLC-MSを用いた毒性バイオマーカーの探索には、種々のモデル化合物を用いた大規模DBの構築、バイオマーカーの同定、さらに得られたバイオマーカーの各代謝経路における意味づけが必要となると考えられるが、尿、あるいは血液のトキシコメタボノミクスは生体への侵襲性が低く、スループットも高いため、今後汎用されてくるものと思われる。

5—おわりに

本稿では、毒性評価の新しいバイオマーカー探索として、遺伝子発現解析、タンパク質発現解析、および内因性代謝物質解析について紹介した。これらのバイオマーカーについて情報を蓄積することで、迅速かつ高感度な生物反応評価の実現、ヒトにおける毒性予測・評価への活用、およびヒトへの外挿へとつながるものと期待される。これらの解析技術単独で毒性評価に貢献することは可能であるが、より総合的な毒性機作理解のためには、従来法である臨床検査、代謝酵素活性等の生化学的アプローチ、病理学的検査から得られたバイオマーカーとも関連付けた総合的な毒性パスウェイ解析（システムズトキシコロジー）がきわめて有効である。しかし、これらの解析手法で生成するデータは膨大であり、従来の手法で得られたデータを含めた全てのデータを同時に解析することは、ハードウェア面でも、また解析ソフトウエア構築面でも容易ではない。現在、毒性評価試験の全てのデータを用いた毒性パスウェイ解析と毒性バイオマーカー探索の共同研究として米国ではFDAのLiver Toxicity Biomarker Study（LTBS）が、欧州ではInnoMed PredToxコンソーシアムが進行しており、従来の評価手法では実験動物で予測不可能であった特異体質性薬剤障害等の副作用予測のための新規バイオマーカー探索に着手している。理想的な毒性バイオマーカーは、検出感度が高いこと、毒性標的組織・発現機作毎の特異性が高いこと、さらにヒトで精度高く毒性予測ができることである。今後の研究の進展により、上述した性格を備えた理想的な毒性バイオマーカーとその測定系が開発されることを期待するものである。

●——参考文献

1) Biomarkers Definitions Working Group: Biomarkers and surrogate endpoints. Preferred definitions and conceptual framework.
Clin Pharmacol Ther 69(3): 89-95, 2001
2) Schena M, Shalon D, Heller R, Chai A, Brown PO, Davis RW: Parallel human genome analysis: microarray-based expression monitoring of 1000 genes.
Proc Natl Acad Sci U S A 93(20): 10614-10619, 1996
3) Kiyosawa N, Ito K, Sakuma K, Niino N, Kanbori M, Yamoto T, Manabe S, Matsunuma N: Evaluation of glutathione deficiency in rat livers by microarray analysis.
Biochem Pharmacol 68(7): 1465-1475, 2004
4) Ruepp SU, Tonge RP, Shaw J, Wallis N, Pognan F: Genomics and proteomics analysis of acetaminophen toxicity in mouse liver.
Toxicol Sci 65(1): 135-150, 2002
5) Fausther M, Villeneuve L, Cadrin M: Heat shock protein 70 expression, keratin phosphorylation and Mallory body formation in hepatocytes from griseofulvin-intoxicated mice.
Comp Hepatol 3(1): 5, 2004
6) Ebbels TM, Keun HC, Beckonert OP, Bollard ME, Lindon JC, Holmes E, Nicholson JK: Prediction and classification of drug toxicity using probabilistic modeling of temporal metabolic data: the consortium on metabonomic toxicology screening approach.
J Proteome Res 6(11): 4407-4422, 2007
7) Soga T, Baran R, Suematsu M, Ueno Y, Ikeda S, Sakurakawa T, Kakazu Y, Ishikawa T, Robert M, Nishioka T, Tomita M: Differential metabolomics reveals ophthalmic acid as an oxidative stress biomarker indicating hepatic glutathione consumption.
J Biol Chem 281(24): 16768-16776, 2006

矢本 敬 やもと・たかし
第一三共株式会社 安全性研究所 第七グループ長
徳島県生まれ
山口大学 農学部卒
山口大学大学院 連合獣医学研究科 博士課程修了
獣医学博士（山口大学大学院）
専門は医薬品の安全性評価、肝毒性、Toxicogenomics

真鍋 淳 まなべ・すなお
第一三共株式会社 安全性研究所 所長
香川県生まれ
東京大学 農学部卒
筑波大学大学院 医科学 修士課程修了
農学博士（東京大学）
専門は医薬品の安全性評価、肝毒性、肺毒性

Available online at www.sciencedirect.com
ScienceDirect
Bioorganic & Medicinal Chemistry Letters 18 (2008) 657–660
Bioorganic & Medicinal Chemistry Letters

Preparation of C_{60}-based active esters and coupling of C_{60} moiety to amines or alcohols

Hiroki Tsumoto,[a,b] Katsumasa Takahashi,[a] Takayoshi Suzuki,[a] Hidehiko Nakagawa,[a] Kohfuku Kohda[b] and Naoki Miyata[a,*]

[a]*Graduate School of Pharmaceutical Sciences, Nagoya City University, 3-1 Tanabedori, Mizuho-ku, Nagoya, Aichi 467-8603, Japan*
[b]*Faculty of Pharmaceutical Sciences, Musashino University, 1-1-20 Shinmachi, Nishitokyo-shi, Tokyo 202-8585, Japan*

Received 22 July 2007; revised 29 October 2007; accepted 17 November 2007
Available online 22 November 2007

Abstract—We report the syntheses of C_{60}-based active esters and the coupling of their C_{60} moiety to various amines or alcohols. Methano[60]fullerene carboxylic acid was activated by esterification with *N*-hydroxysuccinimide (NHS) or pentafluorophenol (PFP) and the active esters were isolated. Reactions of the active esters with amines or alcohols proceeded easily to give a variety of compounds having the C_{60} moiety.

[60]Fullerene derivatives have a wide variety of biological activities such as neuroprotective, enzyme inhibition, photoinduced DNA cleavage, and antigenicity.[1] To apply functionalized fullerenes in material science and medicinal chemistry, many fullerene derivatives have been synthesized by using reactions that involve addition to C_{60}.[2] Methano[60]fullerenes are one of the most well-studied fullerene derivatives, and several methods are available for their synthesis: (i) the Bingel reaction, (ii) the addition–elimination reactions of sulfonium ylides or phosphonium ylides, and (iii) the addition-thermal decomposition of diazo compounds.[3] However, these methods have some limitations in terms of molecular design, namely, method (i) requires strong basic condition, and the preparation of ylides and diazo compounds is difficult in methods (ii) and (iii), respectively. These methods also do not give a pure mono-adduct in high yield due to the formation of isomers and multi-adducts. On the other hand, a series of methano[60]fullerene carboxylic acids are useful to obtain various esters and amides by condensation reactions with alcohols and amines, respectively, using a condensing reagent. Further, the in situ formation of acid chloride from methano[60]fullerene carboxylic acid and the subsequent reaction with alcohol and amine are also useful.[1d,3e,4] However, the carboxylic acid derivatives are insoluble in most organic solvents. Two approaches have been reported to improve solubility. One is the synthesis and isolation of the acid chloride from methano[60]fullerene carboxylic acid, which in turn is converted into amide or ester by reacting with amine or alcohol, respectively.[5] The other is the use of succinimide ester that can react with molecules containing primary and secondary amino groups.[6] The acid chloride and the succinimide ester are both isolable and soluble compounds. Although these methods are convenient, it is difficult to induce the selective reaction of the acid chloride with alcohol or amine due to its high reactivity, forming both ester and amide. Further, the condensation reaction of succinimide ester with alcohol has not been reported.

In this paper, we report a simple and efficient method for the preparation of C_{60} derivatives coupled with amines and alcohols. Methano[60]fullerene carboxylic acid was chosen and its carboxylic acid group was activated to facilitate the formation of the corresponding amide or ester. Condensation reactions using isolated succinimide ester containing C_{60} moiety **1a** have been reported.[6] According to that paper, succinimide ester **1a** was synthesized from fulleromalonic acid $C_{61}(COOH)_2$ and *N*-hydroxysuccinimide (NHS) by the DCCI method with decarboxylation in only 30% yield.[6a] We synthesized **1a** via the condensation reaction of monoacid **1** with NHS using EDCI instead of DCCI, and achieved an improved yield (56%) (Scheme 1). Monoacid **1** was

Keywords: Fullerenes; Amino acids; Peptides; *N*-hydroxysuccinimide esters; Pentafluorophenol esters.
* Corresponding author. Tel./fax: +81 52 836 3407; e-mail: miyata-n@phar.nagoya-cu.ac.jp

prepared from *tert*-butyl [60]fullerene acetate according to the procedure reported in the literature.[3b,c,7] To improve the coupling efficiency of the active ester with amines and alcohols, pentafluorophenol (PFP) ester **1b** was prepared in 71% yield (Scheme 1). PFP ester is highly reactive and is commonly used for the derivatization of primary and secondary amino groups.[8] Furthermore, to obtain various types of intermediates, another type of methano[60]fullerene carboxylic acid **2** was chosen and activated to give active esters **2a** and **2b** in 72% and 91% yields, respectively (Scheme 1). Acid **2** was synthesized from 4-benzoylbutyric acid in four steps according to a procedure reported in the literature.[5a,9] The phenyl ring in **2** has the advantage of further modification, such as introduction of various substituents and replacement of hydrogen with deuterium. Acid **3**, whose phenyl ring hydrogens were converted into deuteriums, was also synthesized from methyl 4-benzoylbutyrate-d_5 **5** in three steps with the procedure used for **2** (Scheme 2). Methyl ester **5** was purchased from Spectra Stable Isotopes, Inc. Acid **4** containing bromo atom was synthesized from methyl 4-(4-bromobenzoyl)butyrate **6** in three steps. Acids **3** and **4** were activated by esterification with NHS or PFP using EDCI in carbon disulfide (CS_2), and active esters **3a**, **4a**, **3b**, and **4b** were isolated in 53%, 67%, 43%, and 91% yields, respectively. These active esters containing the C_{60} moiety were used as the key intermediate to produce a variety of methano[60]fullerene derivatives efficiently.

The derivatization reactions of the isolated active esters toward various amines were demonstrated. First, the active esters were allowed to react with benzylamine to give the corresponding amides **11** (Table 1, entries 1–8). Both NHS ester **1a** and PFP ester **1b** smoothly reacted with benzylamine in quantitative yield (Table 1, entries 1 and 5). In contrast, NHS ester

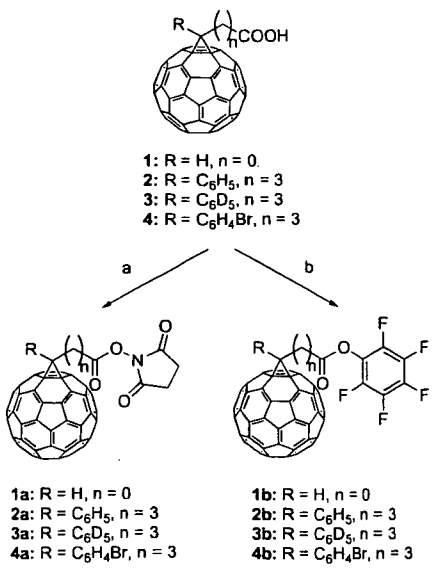

Scheme 1. Syntheses of a series of active esters containing C_{60} moiety from acids **1–4**. Reagents, conditions, and yields: (a) NHS, EDCI, dry THF or CS_2, rt, 53–72%; (b) PFP, EDCI, dry THF or CS_2, rt, 43–91%.

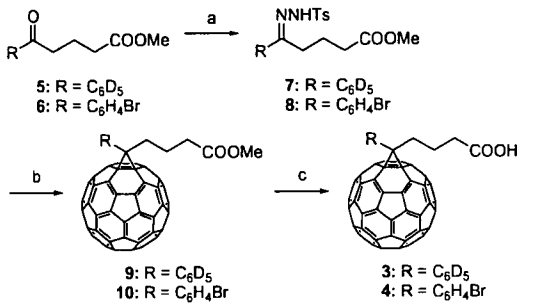

Scheme 2. Syntheses of methano[60]fullerene carboxylic acids **3** and **4**. Reagents, conditions, and yields: (a) $TsNHNH_2$, MeOH, reflux, 81–88%; (b) C_{60}, NaOMe, pyridine, 1,2-dichlorobenzene, reflux, 39–47%; (c) HCl/AcOH, toluene, reflux, 84–94%.

Table 1. Derivatization with amines

Entry	Amine	Active ester	Equiv[a]	Time (h)	Yield (%)
1		**1a**	1.2	2	100
2		**2a**	1.6	2	75
3		**2a**	0.1	1	100[b]
4	H_2N	**4a**	1.0	9	97
5		**1b**	1.4	1	92
6		**2b**	1.6	25	48
7		**2b**	0.1	1	54[b]
8		**4b**	1.0	17	73
9		**1a**	0.1	19	81[b]
10		**2a**	0.1	42	89[b]
11	H_2N COOEt	**1b**	0.1	22	76[b]

[a] Equivalent amount of active ester to amine.
[b] The isolated yield is based on the amount of active ester.

2a reacted in moderate yield (Table 1, entry 2); however, the yield was improved by the reaction with 10 equiv of amine (Table 1, entry 3). Although PFP esters were synthesized to achieve high reactivity to amines, PFP esters **2b** and **4b** were less reactive than NHS esters **2a** and **4a** (entries 2–4 and 6–8). These results are not consistent with our expectation that PFP ester is more reactive than NHS ester. Next, the derivatization with amino acid derivative (10 equiv) was carried out to give the corresponding amides in moderate yields (Table 1, entries 9–11).

To investigate the reactivity of the active esters to alcohol, the derivatization reactions with benzyl alcohol (10 equiv) were carried out using NHS ester **1a** or PFP ester **1b**. Under the same conditions as those used for benzylamine, corresponding ester **12** was not obtained. However, on adding DMAP (1 equiv) to the reaction mixture, the esterification was facilitated to give corresponding ester **12** in 72% and 100% yields, respectively (Fig. 1). Even when a mixture of benzylamine (10 equiv) and benzyl alcohol (10 equiv) was allowed to react with NHS ester **1a** or PFP ester **1b**, only corresponding amide **11** was obtained in 100% and 85% yields, respectively. On the other hand, in the presence of DMAP, a mixture of amide **11** and ester **12** was obtained at the ratio of

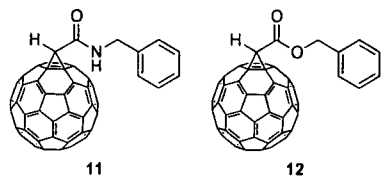

11 12

Figure 1. Structures of compounds **11** and **12**.

12:1. These results demonstrate that the active esters selectively react with amine in the absence of DMAP.

Among the different classes of fullerene derivatives, fullerenes coupled with amino acids or peptides are interesting molecules for biological applications.[4a,6b,10] In this regard, there is a need to develop efficient methods for the preparation of fullerenes coupled with amino acids or peptides to widen the applications of fullerenes. We demonstrate here the derivatization of fullerenes with various amino acids and peptides, which involves the following steps. A solution of the NHS ester in DMF was added to an aqueous solution of amino acids or peptides. The reaction mixture was stirred with vortex mixer for 10 s, left at room temperature for 1–6 h, and subjected to matrix-assisted laser desorption/ionization time-of-flight (MALDI-TOF) mass spectrometry (MS) analysis without further purification. The MALDI-TOF-MS were acquired in the negative ion mode using α-cyano-4-hydroxycinnamic acid (CHCA) as the MALDI matrix. The results of the MALDI-TOF-MS analysis summarized in Table 2 indicate that the NHS esters reacted with the free amino functionality of amino acids and peptides under mild conditions. A typical MALDI-TOF-MS is shown in Figure 2(a). Leucine-enkephalin (YGGFL) was derivatized with NHS ester **1a**. M^- ion of the derivatized peptide was observed at *m/z* 1315.16 (calcd mass: 1315.26). Signals which appeared at *m/z* 600–800 were those derived from the matrix and the reagent. Figure 2(b) shows the reverse-phase HPLC chromatogram of the reaction mixture at 6 h after reaction, which was obtained with a C_4 RP column. The native peptide (4.1 min) was not detected while the derivatized peptide with **1a** was detected at 24.1 min. The broad peak at 26–31 min was derived from the unreacted reagent **1a**. The results of MALDI-TOF-MS analysis and RP-HPLC analysis indicated that NHS ester **1a** reacted with pentapeptide quantitatively.

Table 2. Derivatization with amino acids and peptides

Entry	Amino acid and peptide	Active ester	Monoisotopic MW of derivative	
			Expected	Observed
1	Gly	**1a**	835.03	835.02
		2a	953.11	953.12
		3a	958.14	958.11
		4a	1031.02	1031.03
2	Gly-Gly-Gly	**1a**	949.07	948.94
		2a	1067.15	1067.00
3	Z-Lys	**1a**	1040.14	1040.13
		2a	1158.22	1158.15
4	Bz-Gly-Lys	**1a**	1067.15	1067.16
		2a	1185.23	1185.19
5	Gly-Gly-Tyr-Arg	**1a**	1211.21	1211.04
		2a	1329.29	1329.04
6	Tyr-Gly-Gly-Phe-Leu	**1a**	1315.26	1315.16
		2a	1433.34	1433.10

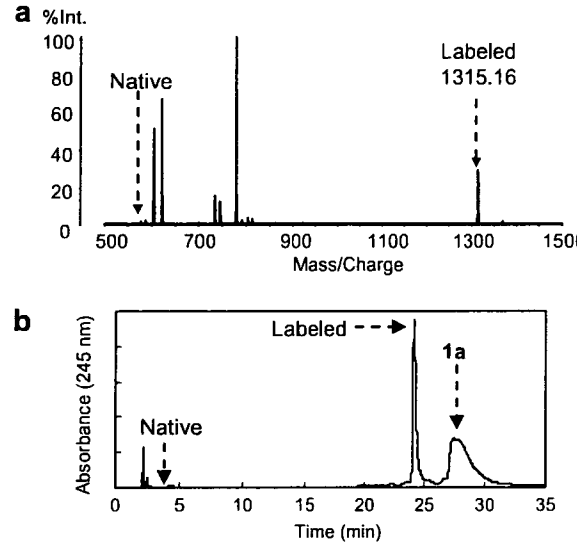

Figure 2. (a) MALDI-TOF-MS of leucine-enkephalin (YGGFL) derivatized with **1a**. M^- ion (calculated mass 1315.26) of the derivatized peptide was observed at *m/z* 1315.16. The spectrum was acquired in the reflectron negative mode using CHCA as the MALDI matrix. (b) RP-HPLC chromatogram of the reaction mixture of YGGFL derivatized with active ester **1a** at 6 h. Inertsil WP300 C_4 column from GL Sciences was used.

Spectral data of new compounds were described in Ref. 11. General procedure for the derivatization with amines was described in Ref. 12.

In summary, NHS esters and PFP esters of methano[60]fullerene carboxylic acids were synthesized and their C_{60} moiety was coupled to molecules containing amino or hydroxyl groups. The active ester reacted with amine selectively and only reacted with alcohol in the presence of DMAP. MALDI-TOF-MS analysis indicated the potential utility of these active esters for the preparation of fullerene-modified amino acids or peptides for application in biological studies. This approach features ease of coupling of the C_{60} moiety to a variety of molecules with amino or hydroxyl groups via a simple reaction under mild conditions. These [60]fullerene-based active esters have the potential to be used as building blocks for the synthesis of various methano[60]fullerene derivatives, extending the application of fullerene in medicinal chemistry and material science. Based on these ideas, expecting the biological activities, we have examined the preparation of some amino acids and related derivatives having C_{60} moiety. Results will be appeared elsewhere soon. Also the applications of our reagents **1a–4a** and **1b–4b** for mass spectrometry of small amine molecules are in progress.

Acknowledgment

This work was partly supported by the Sasakawa Scientific Research Grant from The Japan Science Society.

References and notes

1. (a) Dugan, L. L.; Turetsky, D. M.; Du, C.; Lobner, D.; Wheeler, M.; Almli, C. R.; Shen, C. K.-F.; Luh, T.-Y.; Choi, D. W.; Lin, T.-S. *Proc. Natl. Acad. Sci. U.S.A.* **1997**, *94*, 9434; (b) Friedman, S. H.; De Camp, D. L.; Sijbesma, P. R.; Srdanov, G.; Wudl, F.; Kenyon, G. L. *J. Am. Chem. Soc.* **1993**, *115*, 6506; (c) Tokuyama, H.; Yamago, S.; Nakamura, E.; Shiraki, T.; Sugiura, Y. *J. Am. Chem. Soc.* **1993**, *115*, 7918; (d) Chen, B.-X.; Wilson, S. R.; Das, M.; Coughlin, D. J.; Erlanger, B. F. *Proc. Natl. Acad. Sci. U.S.A.* **1998**, *95*, 10809.
2. (a) Maggini, M.; Scorrano, G.; Prato, M. *J. Am. Chem. Soc.* **1993**, *115*, 9798; (b) Prato, M.; Maggini, M.; Giacometti, C.; Scorrano, G.; Sandona, G.; Farnia, G. *Tetrahedron* **1996**, *52*, 5221; (c) Yamakoshi, Y.; Yagami, T.; Sueyoshi, S.; Miyata, N. *J. Org. Chem.* **1996**, *61*, 7236; (d) Nakamura, E.; Yamago, S. *Acc. Chem. Res.* **2002**, *35*, 867.
3. (a) Bingel, C. *Chem. Ber.* **1993**, *126*, 1957; (b) Wang, Y.; Cao, J.; Schuster, D. I.; Wilson, S. R. *Tetrahedron Lett.* **1995**, *36*, 6843; (c) Bestmann, H. J.; Hadawi, D.; Roder, T.; Moll, C. *Tetrahedron Lett.* **1994**, *35*, 9017; (d) Isaacs, L.; Wehrsig, A.; Diederich, F. *Helv. Chim. Acta.* **1993**, *76*, 1231; (e) Isaacs, L.; Diederich, F. *Helv. Chim. Acta.* **1993**, *76*, 2454.
4. (a) Prato, M.; Bianco, A.; Maggini, M.; Scorrano, G.; Toniolo, C.; Wudl, F. *J. Org. Chem.* **1993**, *58*, 5578; (b) Toniolo, C.; Bianco, A.; Maggini, M.; Scorrano, G.; Prato, M.; Marastoni, M.; Tomatis, R.; Spisani, S.; Palú, G.; Blair, E. D. *J. Med. Chem.* **1994**, *37*, 4558; (c) Giacalone, F.; Segura, J. L.; Martin, N. *J. Org. Chem.* **2002**, *67*, 3529.
5. (a) Hummelen, J. C.; Knight, B. W.; LePeg, F.; Wudl, F.; Yao, J.; Wilkins, C. L. *J. Org. Chem.* **1995**, *60*, 532; (b) Ito, H.; Tada, T.; Sudo, M.; Ishida, Y.; Hino, T.; Saigo, K. *Org. Lett.* **2003**, *5*, 2643.
6. (a) Lamparth, I.; Schick, G.; Hirsch, A. *Liebigs Ann./Recueil* **1997**, *1*, 253; (b) Jung, G.; Redemann, T.; Kroll, K.; Meder, S.; Hirsch, A.; Boheim, G. *J. Peptide Sci.* **2003**, *9*, 784.
7. (a) Sun, Y.-P.; Lawson, G. E.; Riggs, J. E.; Ma, B.; Wang, N.; Moton, D. K. *J. Phys. Chem. A* **1998**, *102*, 5520; (b) Ma, B.; Bunker, C. E.; Guduru, R.; Zhang, X.-F.; Sun, Y.-P. *J. Phys. Chem. A* **1997**, *101*, 5626.
8. Kovacs, J.; Kisfaludy, L.; Ceprini, M. *J. Am. Chem. Soc.* **1967**, *89*, 183.
9. González, R.; Hummelen, J. C.; Wudl, F. *J. Org. Chem.* **1995**, *60*, 2618.
10. (a) Bianco, A.; Da Ros, T.; Prato, M.; Toniolo, C. *J. Pept. Sci.* **2001**, *7*, 208; (b) Pantarotto, D.; Bianco, A.; Pellarini, F.; Tossi, A.; Giangaspero, A.; Zelezetsky, I.; Briand, J.-P.; Prato, M. *J. Am. Chem. Soc.* **2002**, *124*, 12543; (c) Bianco, A.; Pantarotto, D.; Hoebeke, J.; Briand, J.-P.; Prato, M. *Org. Biomol. Chem.* **2003**, *1*, 4141.
11. All the new compounds were characterized on the basis of NMR and mass spectral data. Selected spectroscopic data: **2a**: ^{1}H NMR ($CDCl_3$, 400 MHz, δ; ppm) 7.94 (2H, m), 7.58–7.49 (3H, m), 3.00 (2H, m), 2.85–2.81 (6H, m), 2.31 (2H, m). MALDI-TOF-MS (matrix: CHCA, reflectron negative): calculated molecular ion M^-: 993.10, found M^-: 993.01.
3a: ^{1}H NMR ($CDCl_3$, 500 MHz, δ; ppm) 2.99 (2H, m), 2.85–2.81 (6H, m), 2.31 (2H, m). MALDI-TOF-MS (matrix: CHCA, reflectron negative): calculated molecular ion M^-: 998.13, found M^-: 998.11.
4a: ^{1}H NMR ($CDCl_3$, 500 MHz, δ; ppm) 7.75 (2H, d, J = 8.5 Hz), 7.61 (2H, d, J = 8.5 Hz), 2.90 (2H, t, J = 8.2 Hz), 2.78–2.75 (6H, m), 2.25–2.20 (2H, m). MALDI-TOF-MS (matrix: CHCA, reflectron negative): calculated molecular ion M^-: 1071.01 and $[M+2]^-$: 1073.01, found M^-: 1071.01 and $[M+2]^-$: 1072.99.
1b: ^{1}H NMR ($CDCl_3$, 500 MHz, δ; ppm) 5.09 (1H, s). MALDI-TOF-MS (matrix: CHCA, reflectron negative): calculated molecular ion M^-: 943.99, found M^-: 944.04.
2b: ^{1}H NMR ($CDCl_3$, 500 MHz, δ; ppm) 7.95 (2H, d, J = 7.0 Hz), 7.57 (2H, t, J = 7.3 Hz), 7.49 (1H, t, J = 7.3 Hz), 3.00 (2H, m), 2.88 (2H, t, J = 7.3 Hz), 2.33 (2H, m). MALDI-TOF-MS (matrix: CHCA, reflectron negative) calculated molecular ion M^-: 1062.07, found M^-: 1062.01.
3b: ^{1}H NMR ($CDCl_3$, 500 MHz, δ; ppm) 3.00 (2H, m), 2.88 (2H, m), 2.33 (2H, m). MALDI-TOF-MS (matrix: CHCA, reflectron negative): calculated molecular ion M^-: 1067.10, found M^-: 1067.07.
4b: ^{1}H NMR ($CDCl_3$, 500 MHz, δ; ppm) 7.76 (2H, d, J = 8.5 Hz), 7.63 (2H, d, J = 8.5 Hz), 2.91 (2H, t, J = 8.2 Hz), 2.82 (2H, t, J = 7.3 Hz), 2.26–2.22 (2H, m). MALDI-TOF-MS (matrix: CHCA, reflectron negative): calculated molecular ion M^-: 1139.98 and $[M+2]^-$: 1141.98, found M^-: 1139.22 and $[M+2]^-$: 1141.92.
3: MALDI-TOF-MS (matrix: CHCA, reflectron negative): calculated molecular ion M^-: 901.12, found M^-: 901.08.
4: ^{1}H NMR ($CDCl_3$, 500 MHz, δ; ppm) 7.78 (2H, d, J = 8.5 Hz), 7.64 (2H, d, J = 8.5 Hz), 2.88 (2H, t, J = 8.2 Hz), 2.54 (2H, t, J = 7.3 Hz), 2.20–2.13 (2H, m). MALDI-TOF-MS (matrix: CHCA, reflectron negative): calculated molecular ion M^-: 973.99 and $[M+2]^-$: 975.99, found M^-: 973.99 and $[M+2]^-$: 975.97. **7**: ^{1}H NMR ($CDCl_3$, 500 MHz, δ; ppm) 9.20 (1H, s), 7.92 (2H, d, J = 8.2 Hz), 7.30 (2H, d, J = 8.2 Hz), 3.81 (3H, s), 2.63 (2H, m), 2.41 (3H, s), 2.33 (2H, m), 1.69 (2H, m). MS (EI) *m/z* 379 (M). Mp: 125–126 °C.
8: ^{1}H NMR ($CDCl_3$, 500 MHz, δ; ppm) 9.24 (1H, s), 7.90 (2H, d, J = 8.5 Hz), 7.52 (2H, d, J = 8.5 Hz), 7.46 (2H, d, J = 8.5 Hz), 7.30 (2H, d, J = 8.5 Hz), 3.81 (3H, s), 2.59 (2H, t, J = 8.2 Hz), 2.41 (3H, s), 2.33 (2H, t, J = 6.1 Hz), 1.69–1.64 (2H, m). MS (EI): *m/z* 452 (M), 454 (M + 2). Anal. Calcd for $C_{19}H_{21}BrN_2O_4S$: C, 50.34; H, 4.67; N, 6.18. Found: C, 50.36; H, 4.71; N, 6.08. Mp: 151–155 °C.
9: ^{1}H NMR ($CDCl_3$, 500 MHz, δ; ppm) 3.68 (3H, s), 2.91 (2H, m), 2.53 (2H, t, J = 7.6 Hz), 2.19 (2H, m). MALDI-TOF-MS (matrix: CHCA, reflectron negative): calculated molecular ion M^-: 915.13, found M^-: 915.14.
10: ^{1}H NMR ($CDCl_3$, 500 MHz, δ; ppm) 7.82 (2H, d, J = 8.5 Hz), 7.68 (2H, d, J = 8.5 Hz), 3.69 (3H, s), 2.89 (2H, t, J = 8.5 Hz), 2.54 (2H, t, J = 7.6 Hz), 2.20–2.15 (2H, m). MALDI-TOF-MS (matrix: CHCA, reflectron negative): calculated molecular ion M^-: 988.01 and $[M+2]^-$: 990.01, found M^-: 987.91 and $[M+2]^-$: 989.87.
12. General procedure for the derivatization with amine. To a solution of **2a** (15 mg, 0.015 mmol) in $CHCl_3$ (4 mL) was added 0.18 M solution of benzylamine in $CHCl_3$ (0.85 mL, 0.15 mmol). The reaction mixture was stirred at room temperature for 1 h and then subjected to flash column chromatography on silica gel using a toluene/$CHCl_3$ mixture (1:1) as eluent to give the corresponding amide as a brown solid (16.6 mg, quant). MALDI-TOF-MS (matrix: CHCA, reflectron negative): calculated molecular ion M^-: 985.15, found M^-: 985.10.

Design, Synthesis, Structure−Selectivity Relationship, and Effect on Human Cancer Cells of a Novel Series of Histone Deacetylase 6-Selective Inhibitors

Yukihiro Itoh,[†] Takayoshi Suzuki,*[,†] Akiyasu Kouketsu,[†] Nobuaki Suzuki,[†] Satoko Maeda,[‡] Minoru Yoshida,[‡,§] Hidehiko Nakagawa,[†] and Naoki Miyata*[,†]

Graduate School of Pharmaceutical Sciences, Nagoya City University, 3-1 Tanabe-dori, Mizuho-ku, Nagoya, Aichi 467-8603, Japan. Chemical Genetics Laboratory, RIKEN, Saitama 351-0198, Japan, and CREST Research Project, Japan Science and Technology Agency, Saitama 332-001, Japan

Received July 30, 2007

To uncover novel histone deacetylase 6 (HDAC6)-selective inhibitors and to elucidate the structural requirements for their inhibitory activity, we designed and prepared a series of thiolate analogues based on the structure of an HDAC6-selective substrate and evaluated their properties by Western blotting and enzyme assays. Several thiolate analogues were found to be potent and selective HDAC6 inhibitors. Study of the structure−selectivity relationship revealed that the presence of a bulky alkyl group and *tert*-butylcarbamate group in these compounds is important for HDAC6-selective inhibition. Compounds **16b** and **20b**, the most selective and active compounds in this series, exerted a synergistic inhibition of cancer cell growth in combination with paclitaxel. They also blocked the growth of estrogen receptor α-positive breast cancer MCF-7 cells that had been treated with estrogen. These findings suggested that HDAC6-selective inhibitors have potential as anticancer agents.

Introduction

Reversible protein acetylation is an important post-translational modification that regulates the function of histones and many nonhistone proteins.[1] Acetylation of histone lysine residues is controlled by histone acetyltransferases and histone deacetylases (HDACs[a]) and is closely connected with gene expression and cell cycle progression.[2] The inhibition of HDACs causes histone hyperacetylation and leads to the transcriptional activation of genes such as $p21^{WAF/CIP1}$ and Gadd 45, which are associated with growth arrest and apoptosis in tumor cells.[3] Thus far, 18 HDAC family members have been identified and categorized into two groups, namely, zinc-dependent enzymes (HDAC1−11) and NAD^+-dependent enzymes (SIRT1−7).[2a,4] Among these, HDAC6, one of the zinc-dependent HDAC family members, is unique in that it deacetylates nonhistone proteins, such as α-tubulin, HSP90, and cortactin, and is involved in microtubule stabilization, molecular chaperone activity, and cell motility.[5] Furthermore, recent studies have revealed that HDAC6 is associated with several disease states. It has been reported by Hideshima et al. that the inhibition of HDAC6 causes growth inhibition of multiple myeloma cells without affecting noncancerous cells,[6] and Saji et al. reported that expression of HDAC6 is induced by estrogen stimulation of estrogen receptor α (ERα)-positive breast cancer cells.[7] In addition, HDAC6 inhibition has been reported to be strongly involved in neuroprotection.[8] Therefore, HDAC6-selective inhibitors are of great interest not only as tools for probing the biological functions of the isoform, but also as therapeutic agents having few side effects.

Although a large number of HDAC inhibitors have been found to date,[9] including trichostatin A (TSA, **1**),[10] suberoylanilide hydroxamic acid (SAHA, vorinostat, **2**),[11] trapoxin B (TPX B, **3**),[12] and MS-275 (**4**;[13] Chart 1), most lack HDAC6 selectivity. Most hydroxamate HDAC inhibitors, such as **1** and **2**, exhibit little or no preference for HDAC6, whereas most nonhydroxamate inhibitors, such as **3** and **4**, do not inhibit HDAC6.[5b,c,14] It has been reported that HDAC6 is selectively inhibited by tubacin (**5**; Chart 1), which was discovered by the screening of a 7392 small molecule library.[15] However, there is only limited information on HDAC6-selective inhibitors, and therefore, there is a need to develop novel candidates and to then elucidate their structural requirements for inhibiting HDAC6.

In the course of our study on nonhydroxamate HDAC inhibitors,[14c,16] we found a new class of small molecule thiol-based analogues including NCH-26 (**6**) and NCH-31 (**7**;[16b] Chart 2). Thiols are presumed to inhibit HDACs by coordinating the zinc ion, which is required for deacetylation of the acetylated lysine substrate. Furthermore, the *S*-isobutyryl prodrugs NCH-47 (**8**) and NCH-51 (**9**;[17] Chart 2), which are thought to be hydrolyzed to their free thiol forms within cells, showed potent inhibition of cancer cell growth. Following these findings, we recently performed further investigation of thiolate analogues to uncover those that were HDAC6-selective, and discovered highly potent and selective HDAC inhibitors.[18] In the present report, we describe in full detail the design, synthesis, structure−selectivity relationship, and cellular activity of thiol-based HDAC6-selective inhibitors.

Chemistry

The compounds prepared for this study are shown in Figures 1 and 3 and Table 1. Syntheses were carried out as outlined in Schemes 1−4. The route for synthesis of compounds **11b**−**25b** is described in Scheme 1. (*S*)-2-amino-7-bromoheptanoic acid **42**[19] was treated with $(Boc)_2O$ to yield *N*-Boc compound **43**. Condensation of acid **43** with an appropriate amine afforded amides **11c**−**25c**. Bromides **11c**−**25c** were treated with thio-

* To whom correspondence should be addressed. Tel. and fax: +81-52-836-3407. E-mail: suzuki@phar.nagoya-cu.ac.jp (T.S.); miyata-n@phar.nagoya-cu.ac.jp (N.M.).
† Graduate School of Pharmaceutical Sciences, Nagoya City University.
‡ Chemical Genetics Laboratory, RIKEN.
§ CREST Research Project.

[a] Abbreviations: HDAC, histone deacetylase; SIRT, sirtuin; ERα, estrogen receptor α; TSA, trichostatin A; SAHA, suberoylanilide hydroxamic acid; TPX B, trapoxin B; PTX, paclitaxel; E2, 17β-estradiol.

Chart 1. Examples of HDAC Inhibitors

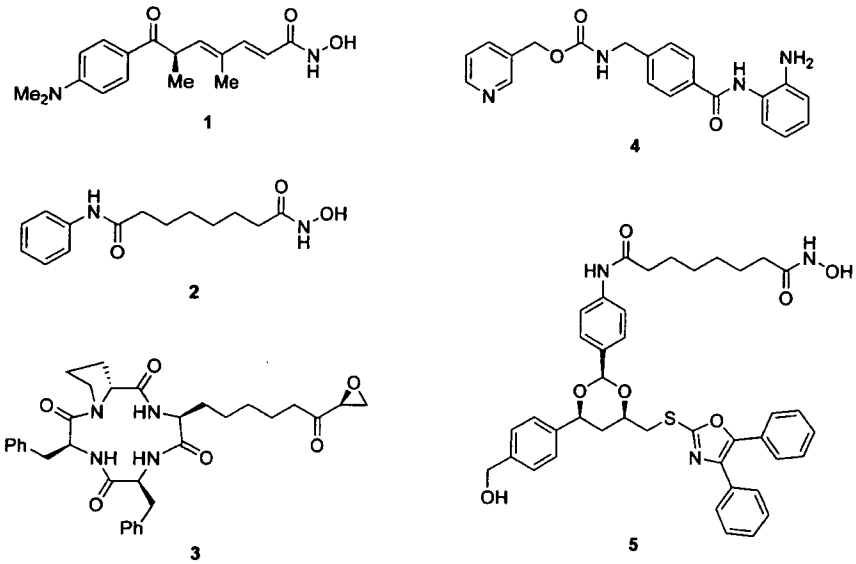

Chart 2. Thiolate HDAC Inhibitors

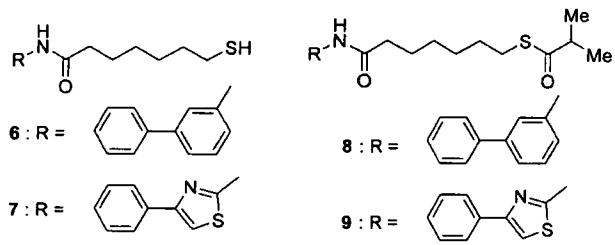

isobutyric acid under alkaline conditions to yield the desired thioesters **11b**–**25b**.

Compounds **26b**–**41b** were synthesized from thioester **16b** by the route shown in Scheme 2. Removal of the Boc group of **16b** gave amine **26b**. Amine **26b** was allowed to react with the corresponding acid chloride, carboxylic acid, chloroformate, isocyanate or thioisocyanate to give **27b**–**41b**.

Compounds **13a**, **15a**–**20a**, and **26a** were prepared from the corresponding bromides **13c** and **15c**–**20c** (Scheme 3). Treatment of the bromides with potassium thioacetate and subsequent hydrolysis of the thioesters gave thiols **13a** and **15a**–**20a**. Deprotection of the Boc group of **16a** gave amine **26a**.

Thiols **27a**, **28a**, **31a**, **33a**, **35a**–**38a**, and **40a** were synthesized from thioester **16d** as outlined in Scheme 4. Thioester **16d** was converted to thiols **27a**, **28a**, **31a**, **33a**, **35a**–**38a**, and **40a** by Boc deprotection of **16d**, treatment of amine **26d** with an appropriate acid chloride, carboxylic acid, chloroformate, isocyanate, or thioisocyanate, and subsequent hydrolysis of thioacetates **27d**, **28d**, **31d**, **33d**, **35d**–**38d**, and **40d**.

Results and Discussion

In designing novel HDAC6-selective inhibitors, we focused initially on small molecule HDAC6-selective substrate **10** (Chart 3), which was discovered by Jung and co-workers.[20] According to their report, compound **10** is selectively deacetylated by HDAC6 in preference to HDAC1 and HDAC3, and the presence of *N*-Boc and trifluoromethyl coumaryl amide in this compound was found to be important for HDAC6 selectivity. This indicated that the structure of *N*-Boc and trifluoromethyl coumaryl amide of compound **10** is selectively recognized by HDAC6, and so, we considered that compound **11a**, in which the acetamide of **10** is replaced by a thiol, might selectively inhibit HDAC6 (Chart 3).

Because HDAC6 has been reported as an α-tubulin deacetylase, inhibition of HDAC6 and that of other HDACs can be assessed according to the accumulation of acetylated α-tubulin and acetylated histones, respectively, using Western blot analysis. We initially evaluated the histone H4/α-tubulin acetylation selectivity of compounds **2**, **8**, **9**, and **11b**, the *S*-isobutyryl prodrug of **11a**, using Western blot analysis (Figure 2). As expected, compound **11b** seemed to induce the accumulation

Scheme 1[a]

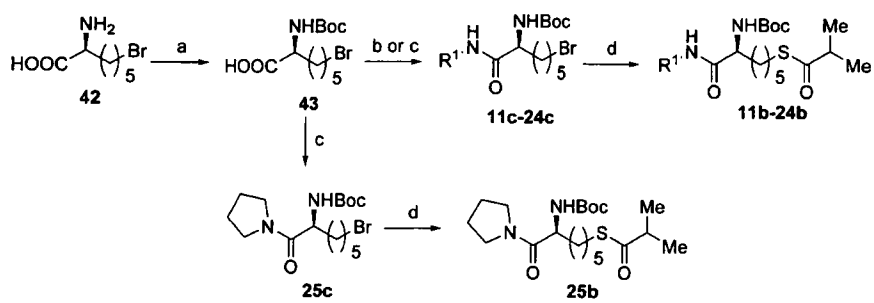

[a] Reagents and conditions: (a) $(Boc)_2O$, Et_3N, THF, H_2O, rt, 95%; (b) R^1NH_2, $POCl_3$, pyridine, −15 °C, 10–48%; (c) R^1NH_2, 1-ethyl-3-(3-dimethylaminopropyl)carbodiimide (EDCI), 1-hydroxybenzotriazole hydrate (HOBt·H_2O), THF, rt, 69–93%; (d) thioisobutyric acid, Et_3N, EtOH, rt, 19–100%.

Scheme 2[a]

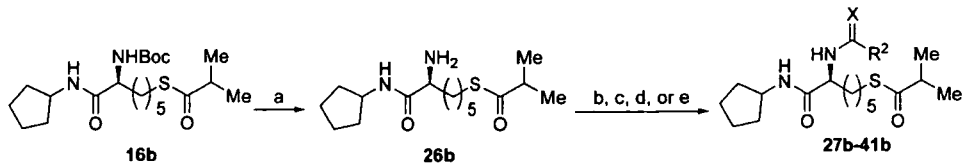

[a] Reagents and conditions: (a) HCl, AcOEt, rt, 100%; (b) R^2COCl, Et_3N, CH_2Cl_2, rt, 11−74%; (c) $(R^2CO)_2O$, 4-dimethylaminopyridine (DMAP), Et_3N, CH_2Cl_2, rt, 52%; (d) R^2COOH, EDCI, $HOBt{\cdot}H_2O$, DMF, 28−62%; (e) R^2NCX, Et_3N, CH_2Cl_2, rt, 24−76%.

Scheme 3[a]

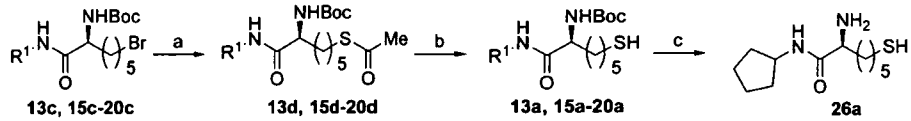

[a] Reagents and conditions: (a) KSAc, EtOH, rt, 57−93%; (b) NaOH, H_2O, EtOH, rt, 53−77%; (c) HCl, AcOEt, rt, 94%.

Scheme 4[a]

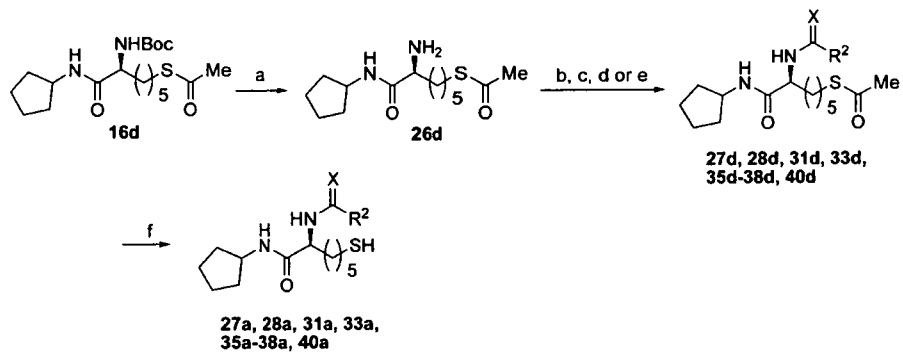

[a] Reagents and conditions: (a) HCl, AcOEt, rt, 100%; (b) R^2COCl, Et_3N, CH_2Cl_2, rt, 26−91%; (c) $(R^2CO)_2O$, DMAP, Et_3N, CH_2Cl_2, rt, 52%; (d) R^2COOH, EDCI, $HOBt{\cdot}H_2O$, DMF, 60%; (e) R^2NCX, Et_3N, CH_2Cl_2, rt, 39−95%; (f) NaOH, H_2O, EtOH, rt, 63−100%.

Chart 3. Design of HDAC6-Selective Inhibitors

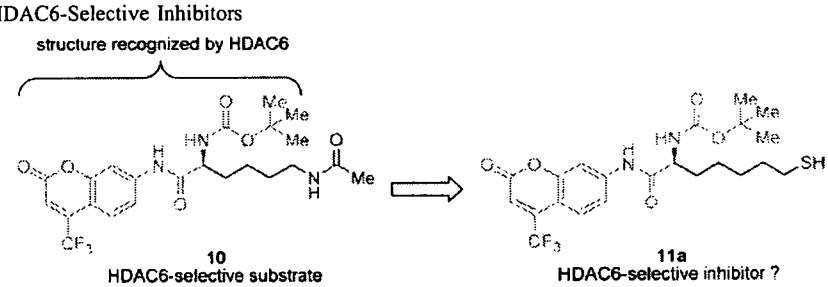

of acetylated α-tubulin as compared with **2**, **8**, and **9**, which did not have this effect. To obtain highly more selective compounds, the coumarin structure of **11b** was converted to analogs with various functional groups (**12b**−**25b**; Figure 1), and these were examined for their selectivity. Compounds **12b**−**15b** and **21b**, with an aromatic ring, compounds **22b**−**24b**, with a smaller hydrophilic group, and compound **25b**, with a tertiary amide group, did not show high selectivity, whereas compounds **16b**−**20b**, in which R^1 = a bulky alkyl group, induced a dose-dependent increase in α-tubulin acetylation but no major increase in acetylated histone H4 (Figure 2). These results indicated that compounds **16b**−**20b** selectively inhibit HDAC6 in preference to nuclear HDACs in cells.

Having investigated the requirements for the R^1 group (Figures 1 and 2), we next turned our attention to the replacement of the *N*-Boc group (Figures 3 and 4). We employed the cyclopentyl group as the R^1 group and determined the effect of replacement of the *N*-Boc group with other functional groups. We initially evaluated amine **26b** in which the Boc group of **16b** is removed, however, **26b** induced neither histone H4 acetylation nor α-tubulin acetylation. Next, we tested aromatic amides (**27b**−**29b**). Among these, phenyl amide **27b** induced the acetylation of α-tubulin, but its selectivity seemed to decrease when compared with that of the lead compound **16b**. We also examined aliphatic amides (**30b**−**34b**). Although hydroxymethyl compound **30b** was found to be a highly potent α-tubulin acetylating agent, its selectivity seemed to be low as compared with **16b**. Compounds **31b** and **32b** caused the accumulation of both acetylated histone H4 and acetylated α-tubulin, whereas compounds **33b** and **34b** only displayed a weak acetylation activity. It is remarkable that neopentyl amide **34b** did not show any α-tubulin acetylating activity or selectivity at all. In other words, replacement of the oxygen atom of the Boc group with a methylene group significantly decreased both potency and selectivity. This suggests that the carbamate group is important for α-tubulin acetylation selectivity. To confirm the importance of the carbamate structure, we replaced the carbamate group of **16b** with urea (**35b**) and thiourea (**36b**) and

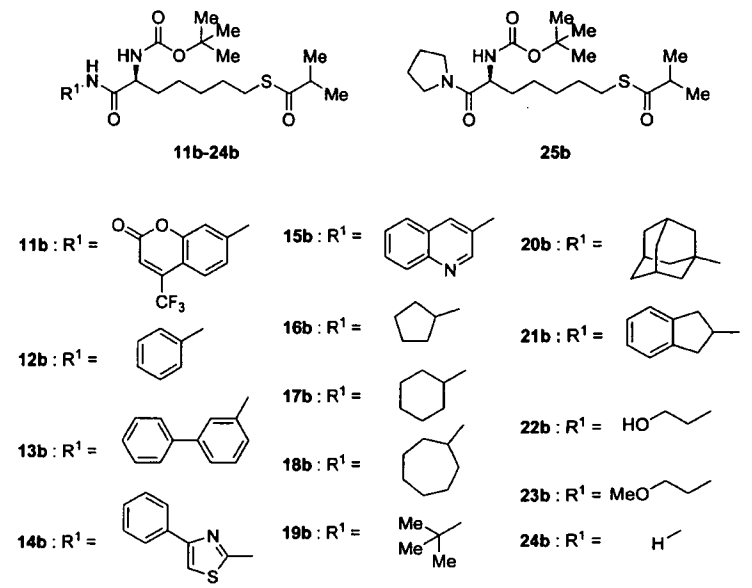

Figure 1. Structures of **11b–25b**.

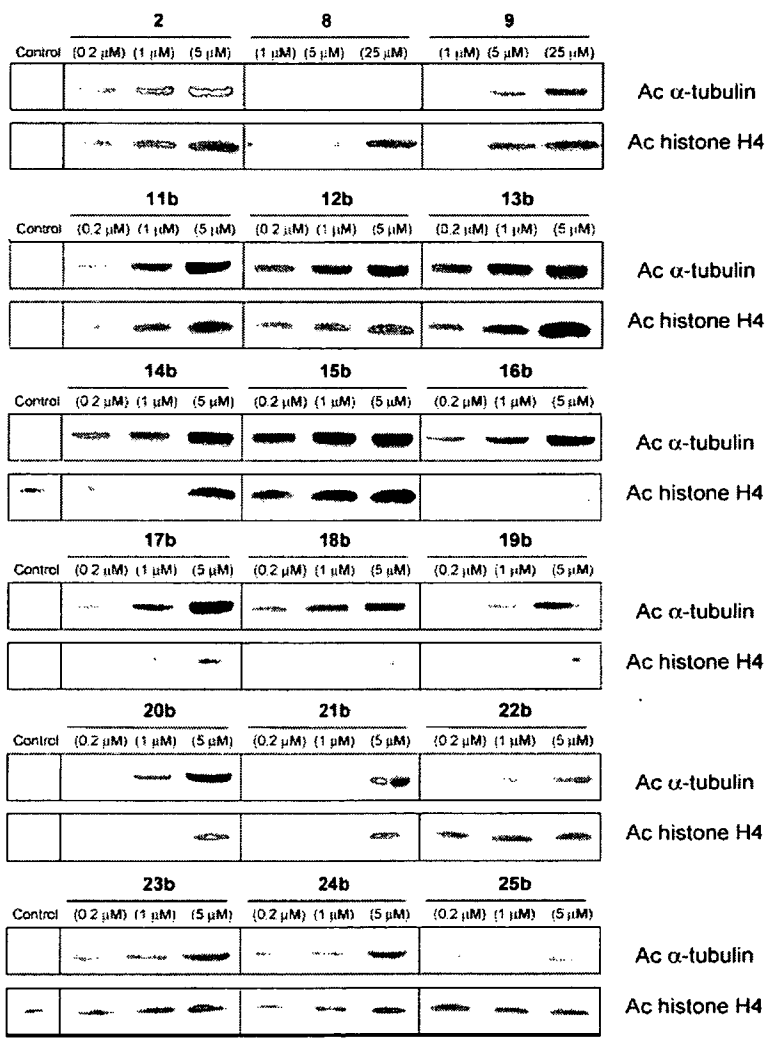

Figure 2. Western blot detection of acetylated α-tubulin and acetylated histone H4 levels in HCT116 cells after 8 h treatment with **2**, **8**, **9**, and **11b–25b**.